



LIQUID CRYSTALLINE ACHIRAL FERROELECTRIC MATERIALS

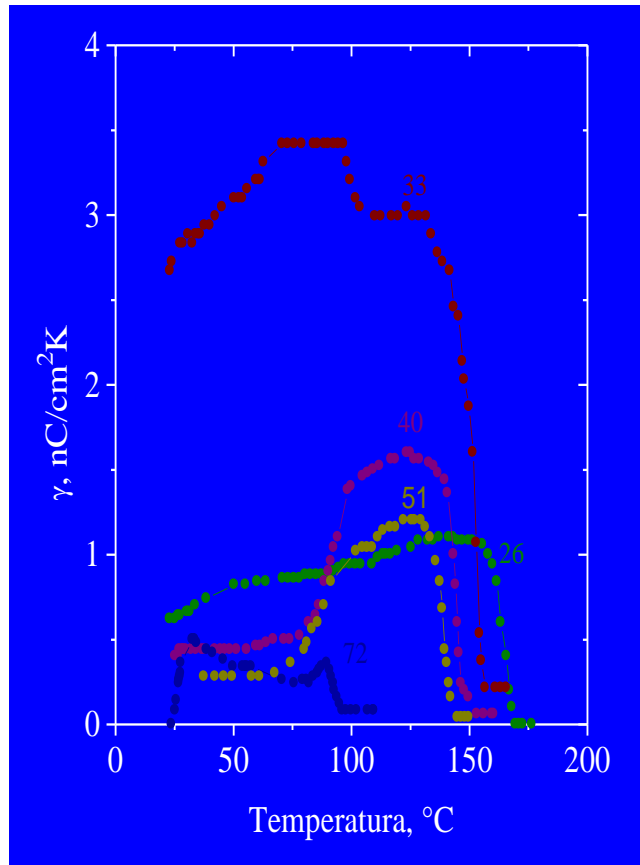
**E. A. Soto Bustamante*, R. Vergara-Toloza, C. M. González Henriquez,
G.A. Rodríguez Leyht, D. Saldaño Hurtado**

**Universidad de Chile, Facultad de Ciencias Químicas y
Farmacéuticas, Departamento de Química Orgánica y Físico Química**

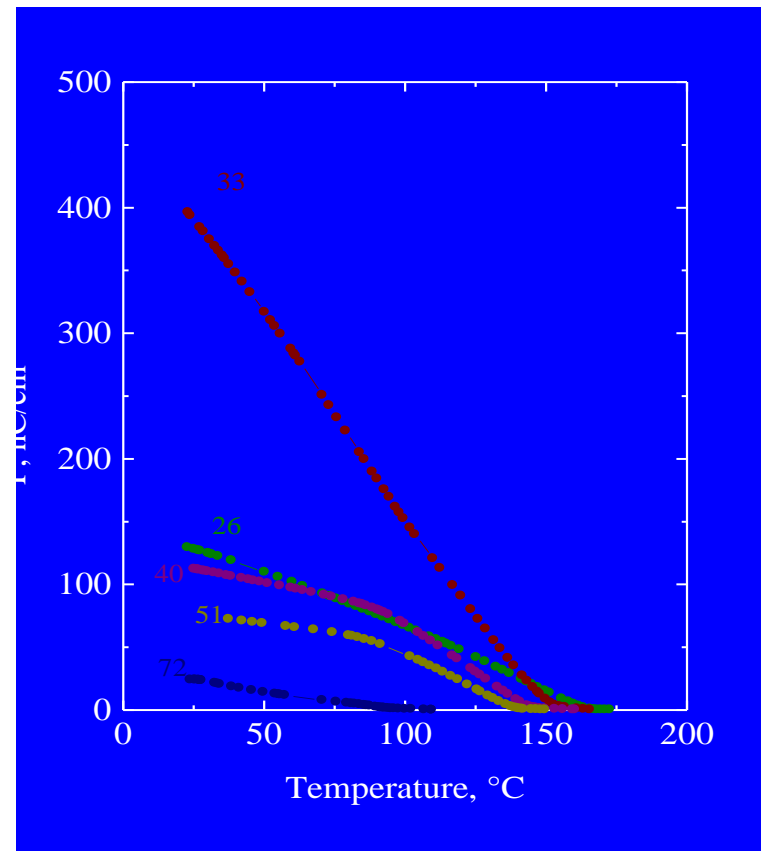
Pyroelectric measurements in PM6R8 mixtures

By cooling under an applied electric field

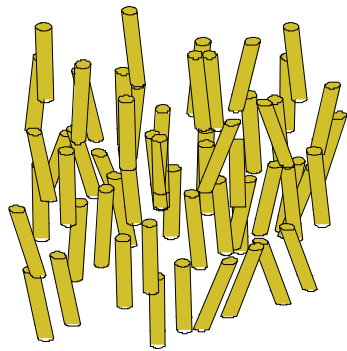
Pyroelectric curve



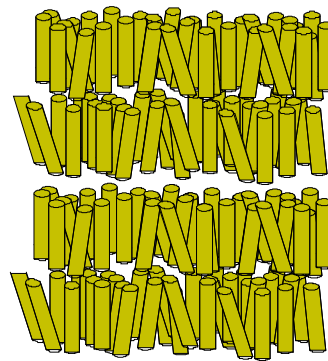
Macroscopic polarization



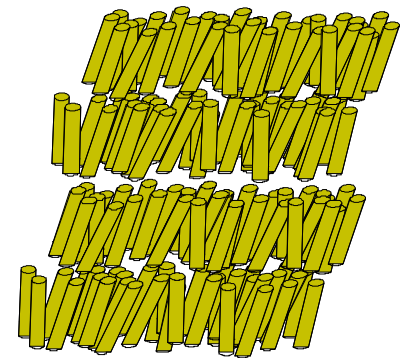
Nematic



Smectic A

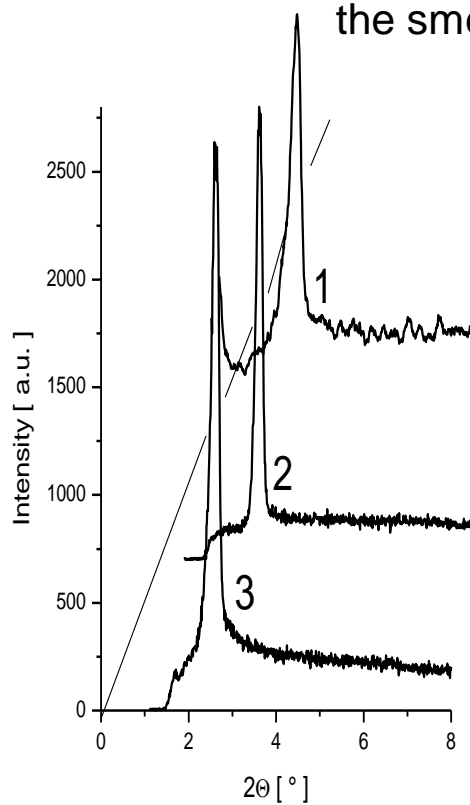


Smectic C

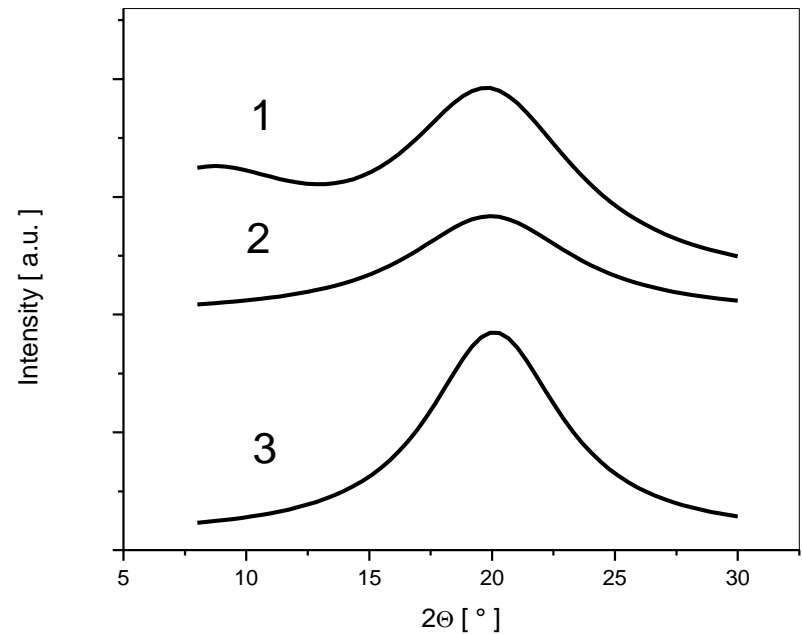


X-Ray Diffraction for monomers

Small angles region at 80 °C: (1) M4R5, (2) M4R6 and (3) M4R8 in the smectic A phase.



Wide angle region showing diffuses halos. The solid lines corresponds to the statistic correlation.



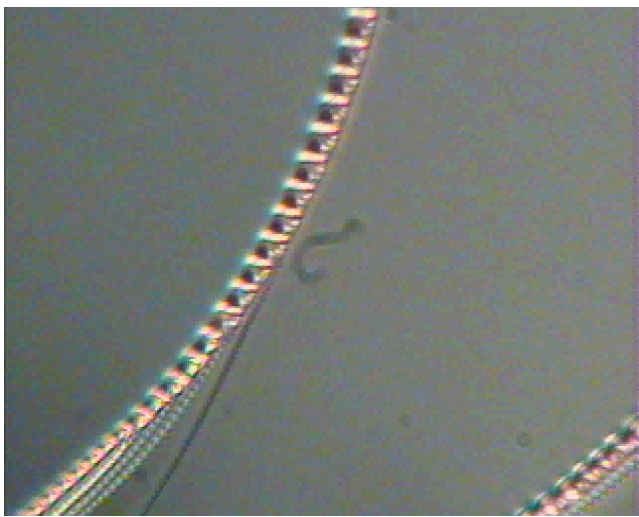
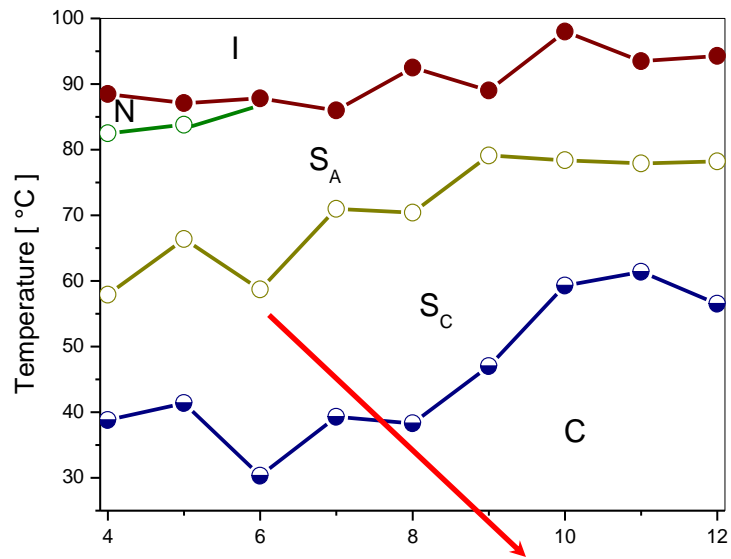
Phase transitions and enthalpy for monomers

Sample	Mesophase	Enthalpy [KJ/mol]
M4R4	C – 38.8 – S _C – 57.9 – S _A – 82.5 – N – 88.5 – I	30.25 – n.d. – 2.08 – 4.76
M4R5	C – 41.4 – S _C – 66.4 – S _A – 83.8 – N – 87.1 – I	45.00 – n.d. – 2.50 – 1.54
M4R6	C – 30.3 – S _C – 58.7 – S _A – 87.8 – I	45.66 – n.d. – 5.12
M4R7	C – 39.3 – S _C – 71.0 – S _A – 86.0 – I	48.52 – n.d. – 6.63
M4R8	C – 38.3 – S _C – 70.4 – S _A – 92.5 – I	50.26 – n.d. – 6.83
M4R9	C – 47.0 – S _C – 79.1 – S _A – 89.0 – I	50.84 – n.d. – 7.03
M4R10	C – 59.3 – S _C – 78.4 – S _A – 98.0 – I	56.09 – n.d. – 7.23
M4R11	C – 61.4 – S _C – 77.9 – S _A – 93.5 – I	60.25 – n.d. – 6.90
M4R12	C – 56.5 – S _C – 78.2 – S _A – 94.3 – I	59.12 – n.d. – 7.95
M6R6	C – 60.0 – S _C – 69.0 – S _A – 96.4 – I	38.72 – n.d. – 5.53
M6R7	C – 51.4 – S _C – 69.8 – S _A – 91.4 – I	27.72 – n.d. – 5.00
M6R8	C – 54.7 – S _C – 80.0 – S _A – 97.9 – I	39.38 – n.d. – 5.80
M6R9	C – 55.2 – S _C – 70.2 – S _A – 91.3 – I	29.29 – n.d. – 6.01
M6R10	C – 48.3 – S _C – 83.3 – S _A – 96.6 – I	30.02 – n.d. – 6.82
M6R11	C – 58.1 – S _C – 74.6 – S _A – 92.0 – I	41.99 – n.d. – 7.27
M6R12	C – 46.1 – S _C – 87.9 – S _A – 96.6 – I	33.28 – n.d. – 7.12

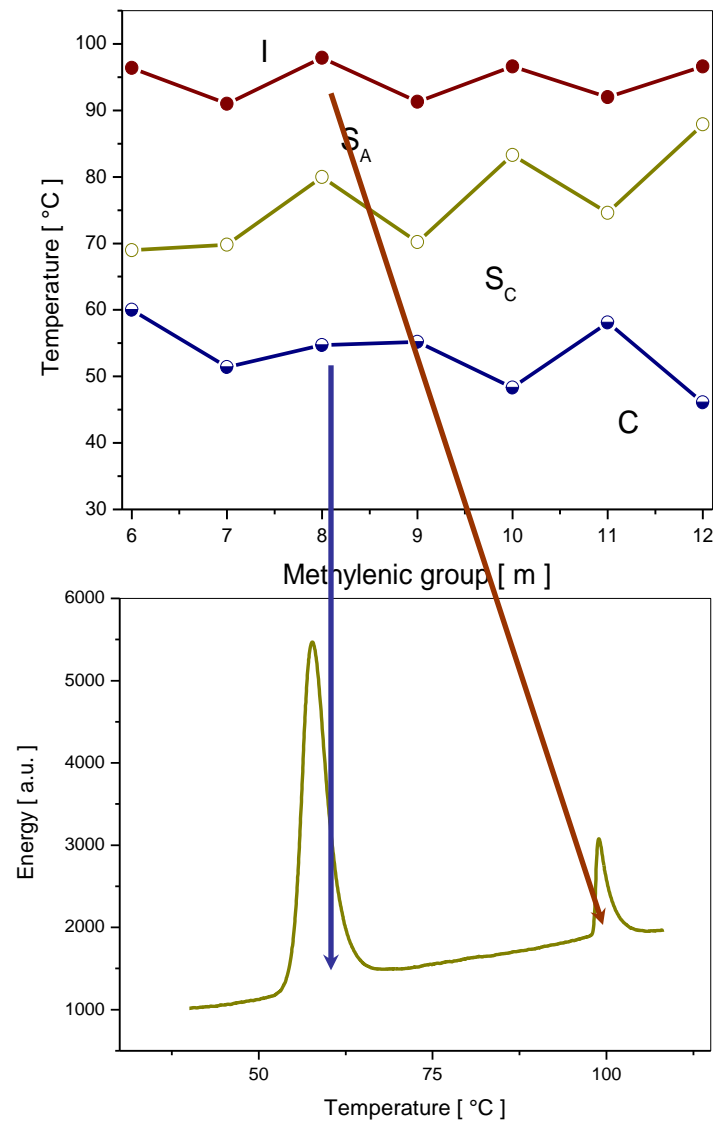
n.d. : Non determined

Phase diagrams by cooling

M4 Serie

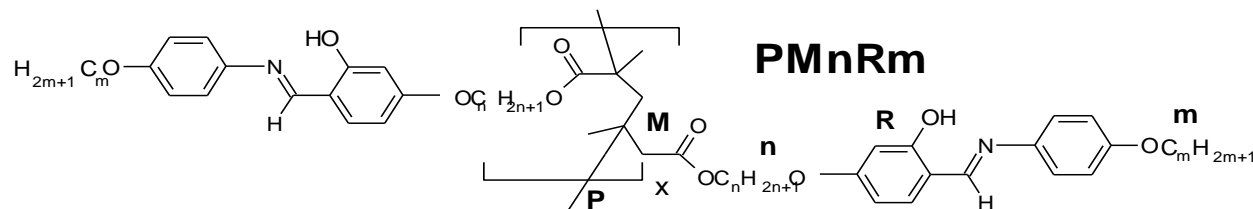


M6 Serie



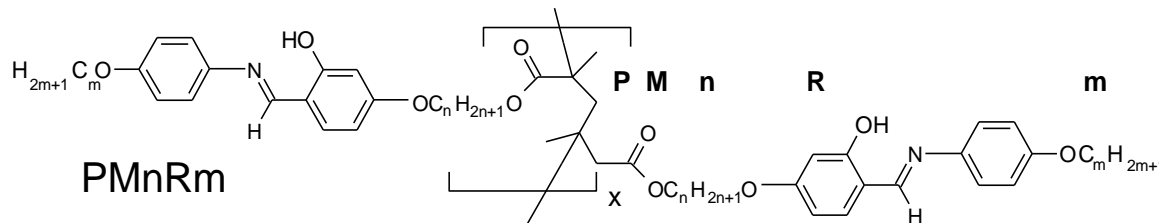
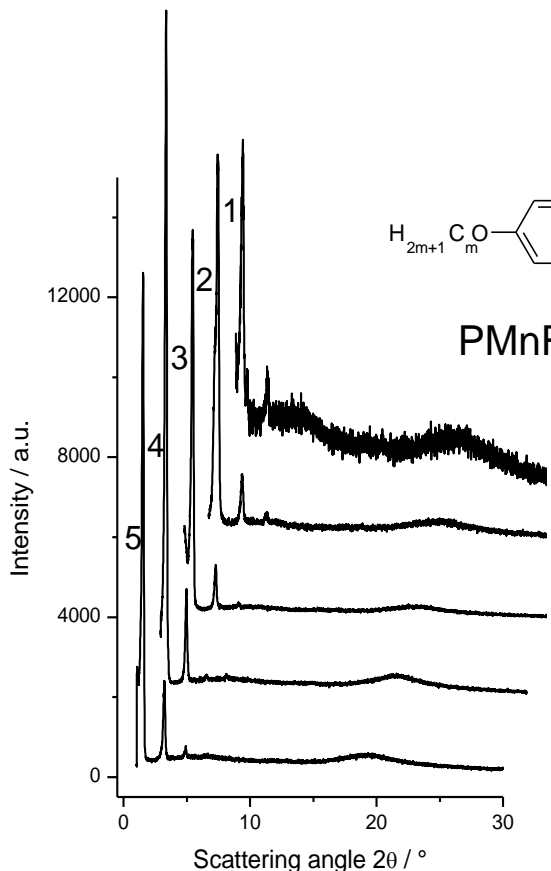
Polymer Characterization

Phase transition Temperature, entalpy and molecular weigth characterization Mw and Mn



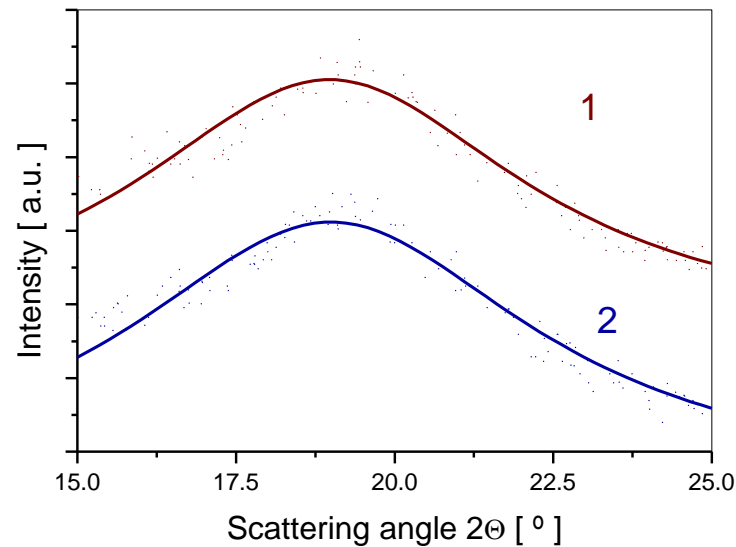
Sample	Mesophase	Entalpy [J/g]	\bar{M}_w [g / mol]	<i>DI</i>	<i>P_w</i>
PM4R5	g – 50.8 – S _{C2} – 187.1 – I	21.97	124,813	1.703	284
PM4R6	g – 58.7 – S _{C2} – 191.3 – I	13.80	86,229	1.786	190
PM4R8	g – 57.8 – S _{C2} – 201.3 – I	15.62	129,607	1.193	269
PM6R6 ^[7]	g – 82.0 – S _{C2} – 157.0 – S _{Ad} – 173.0 – I	10.30/ 4.32	77,575	1.756	161
PM6R7	g – 83.4 – S _{C2} – 162.7 – S _{Ad} – 176.7 – I	7.78/2.70	55,126	1.313	111
PM6R8 ^[12]	g – 82.0 – S _{C2} – 180.0 – I	16.40	81,500	2.100	160
PM6R9	g – 62.2 – S _{C2} – 183.6 – I	18.55	115,209	1.313	220
PM6R10 ^[9]	g – 64.2 – S _{C2} – 190.3 – I	19.02	104,300	2.370	194
PM6R11	g – 70.6 – S _{C2} – 195.3 – I	19.45	102,016	1.587	185
PM6R12 ^[9]	g – n.d. – S _{C2} – 190.5 – I	21.20	108,100	2.609	191

X-Ray Diffraction

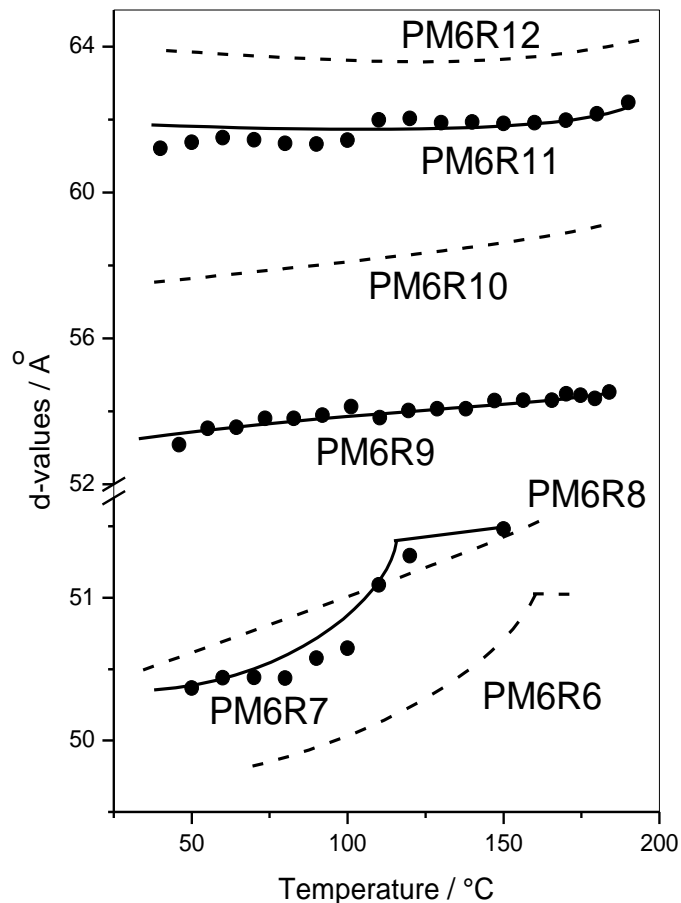


(1) PM4R5 at 190 °C, (2) PM4R6 at 160 °C, (3) PM4R8 at 120°C, (4) PM6R9 at 125 °C and (5) PM6R11 at 170 °C. The (001) reflex position corresponds to a bilayer structure.

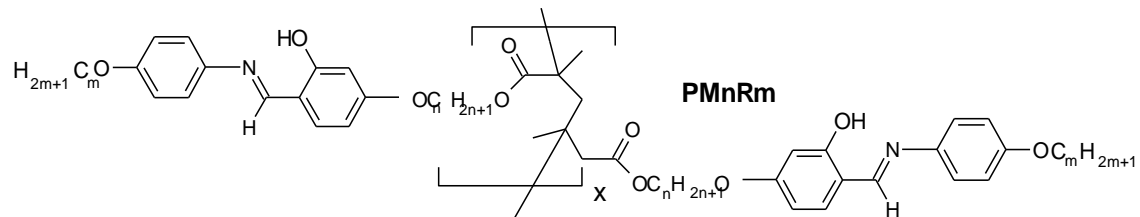
Difuse halos correspond to the distance average for the intermolecular distance D in the smectic phase, showing a liquid like packing.



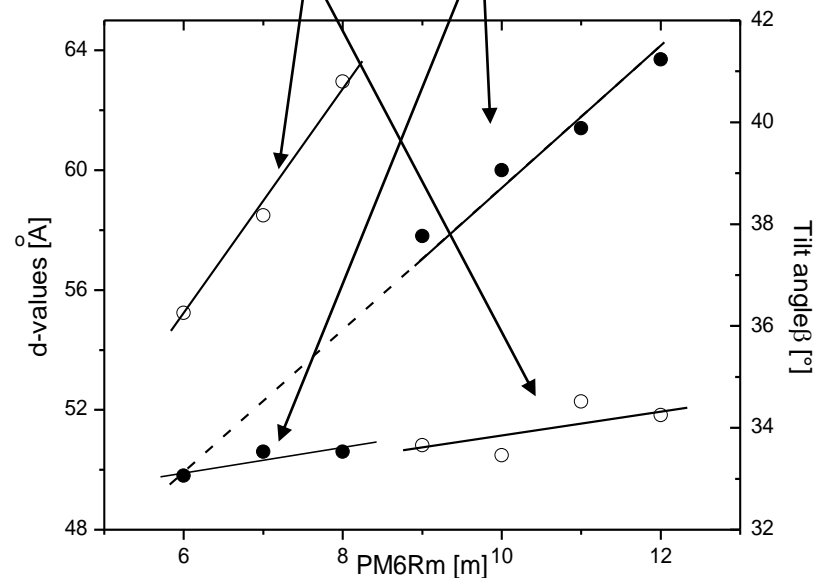
Interlayer distance temperature dependence



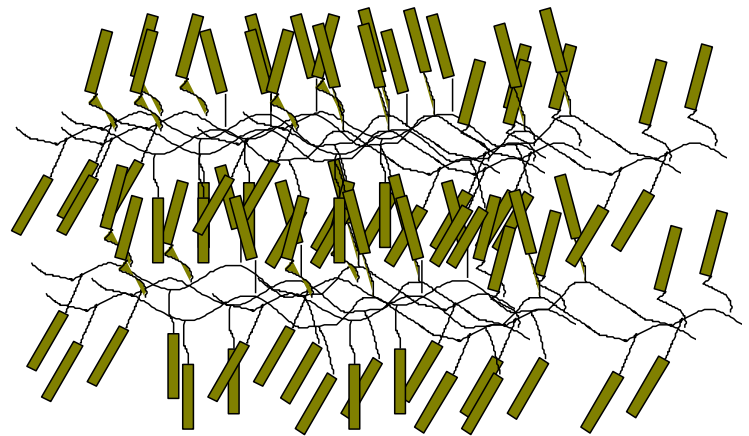
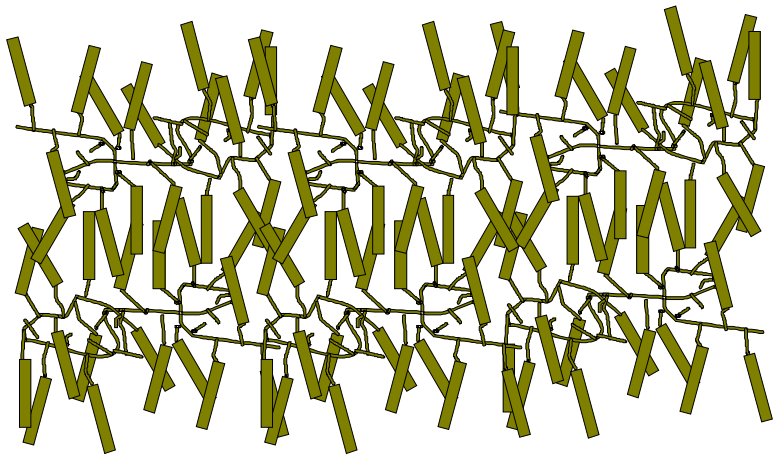
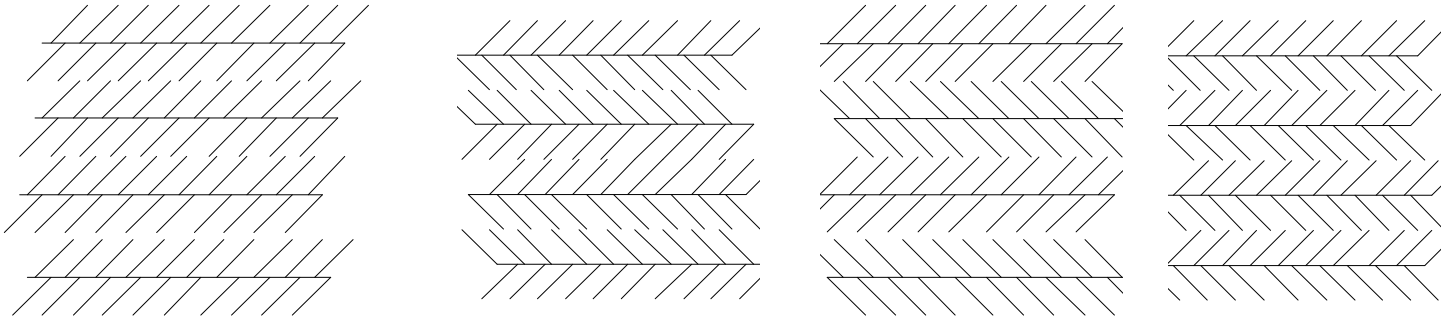
Interlayer distance temperature dependence by cooling



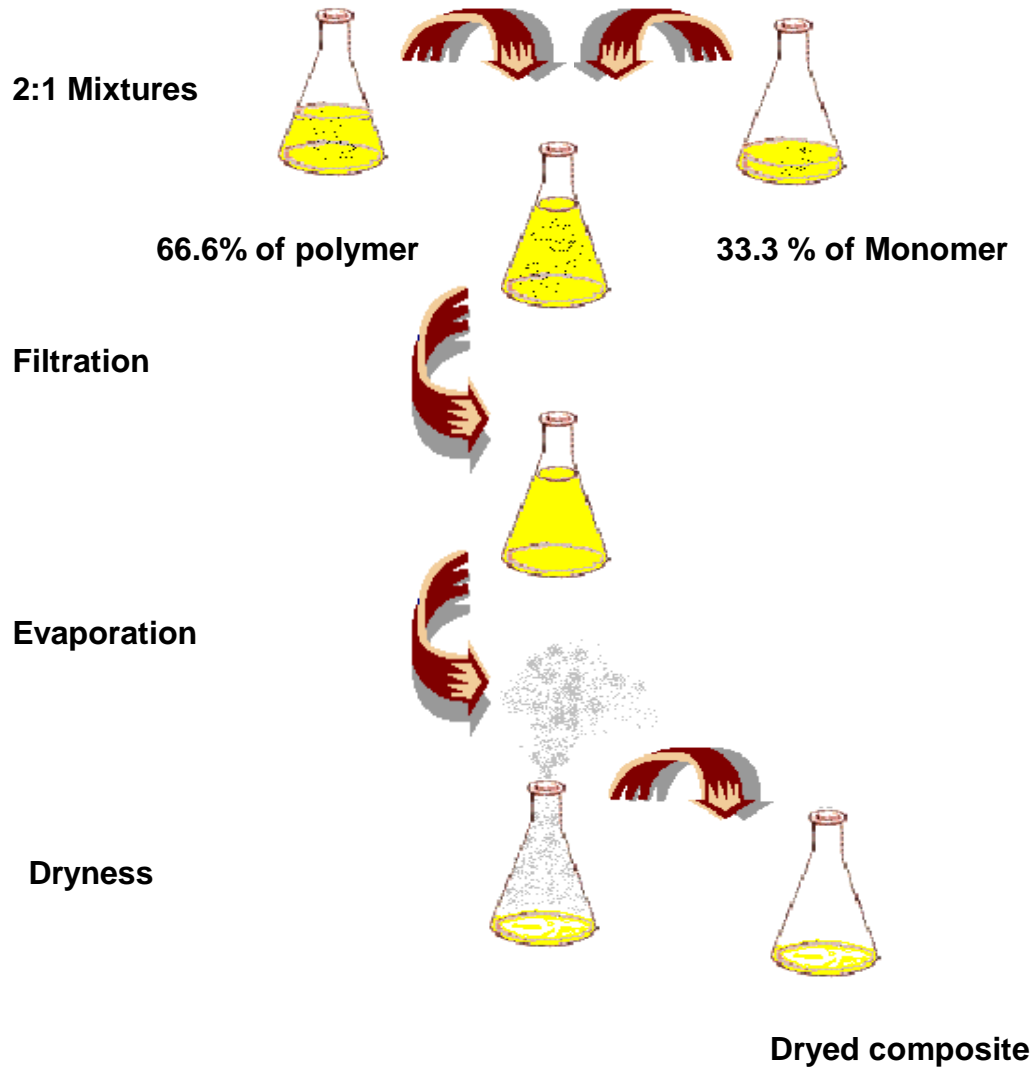
Interlayer distance d (full circle) and tilt angle β (open circles) in the smectic C2 phase at 80 °C against the mesogenic group length.



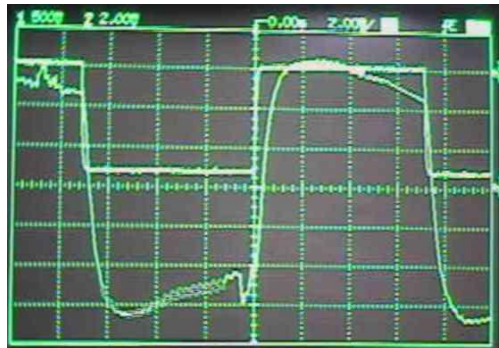
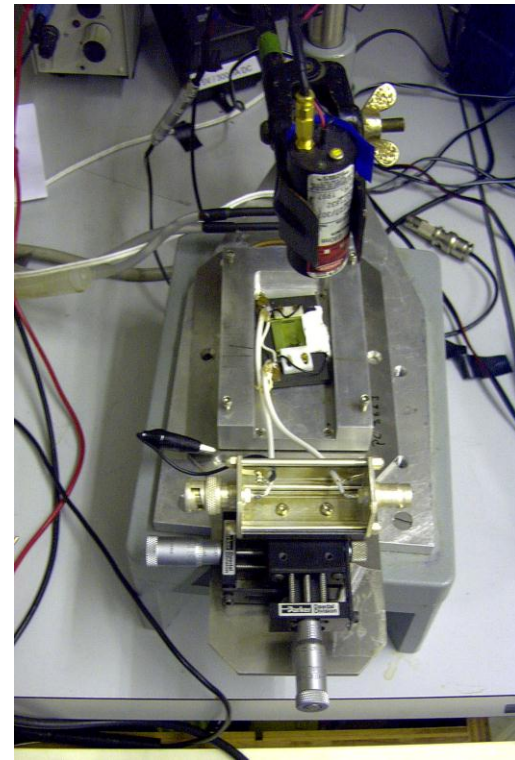
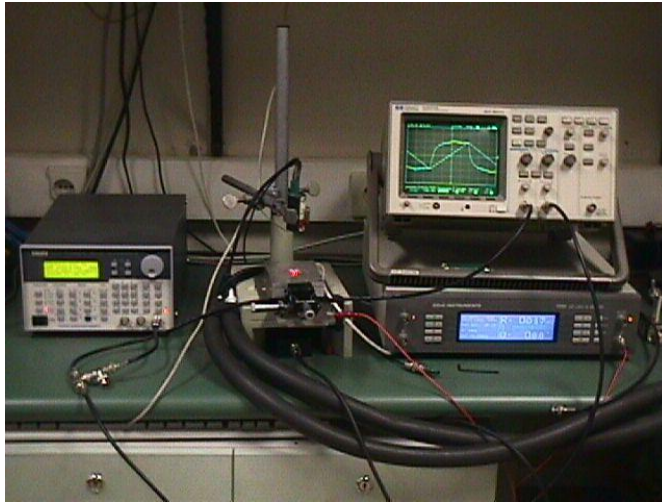
Smectic C2 phase in a polymer



Composites Preparation

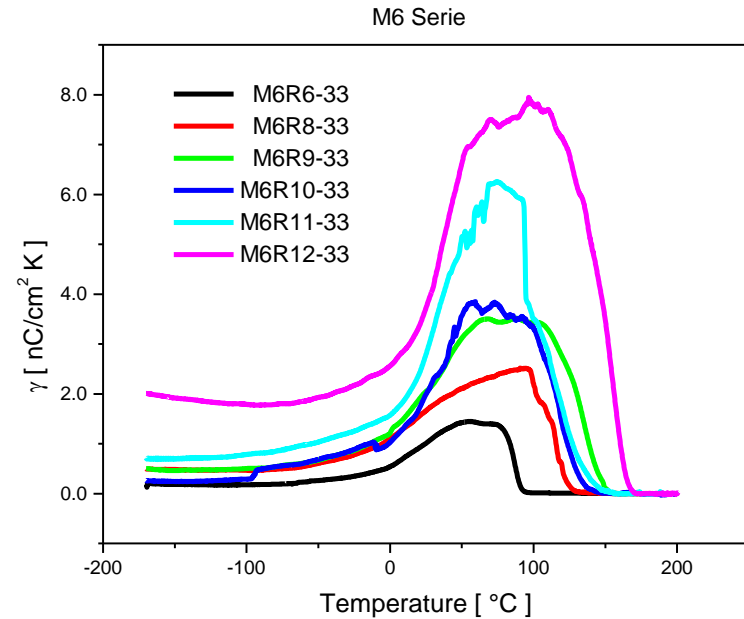
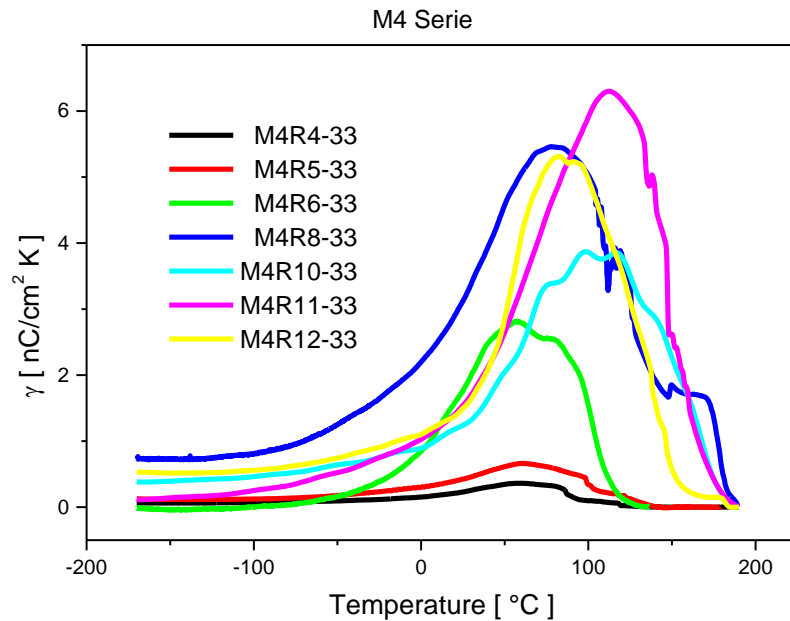


Pyroelectric modulated technique



Pyroelectric studies

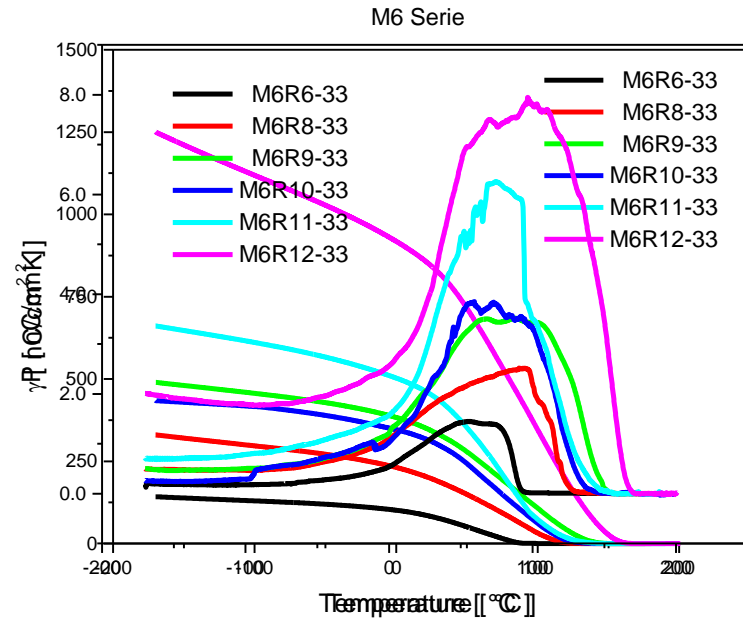
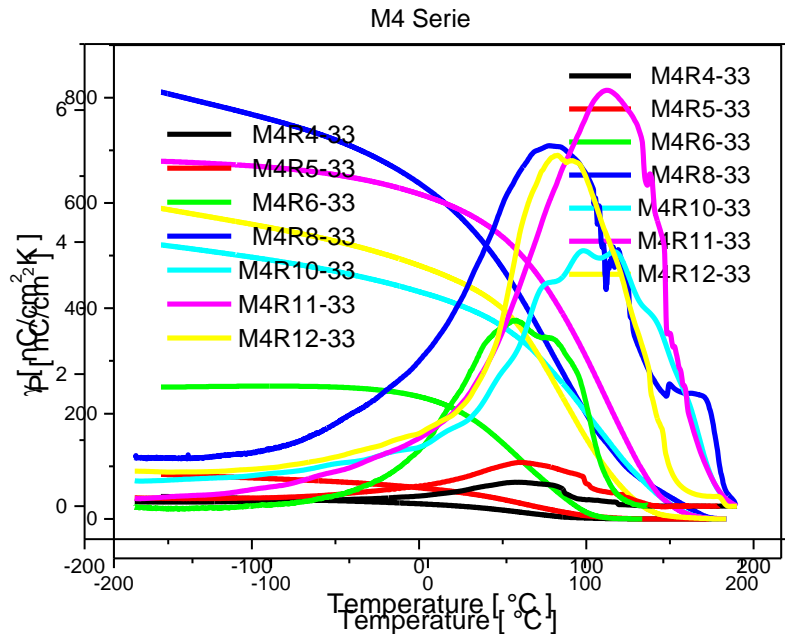
In previously poled samples: from -170 °C until the isotropic state. (10 V/ μ m).

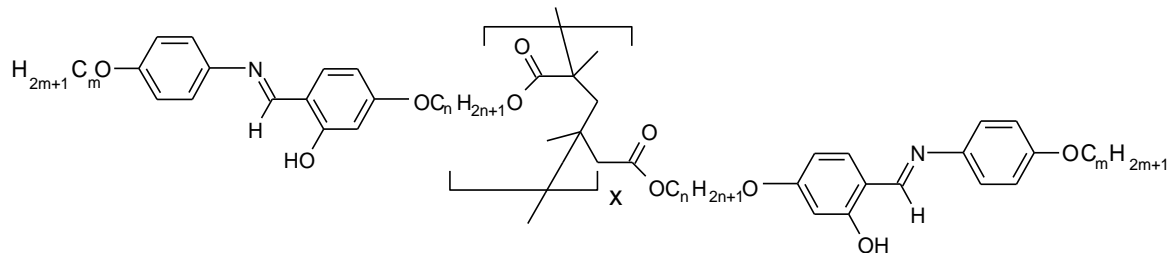


Pyroelectric answer for M4Rn-33 and PM6Rn-33 Serie

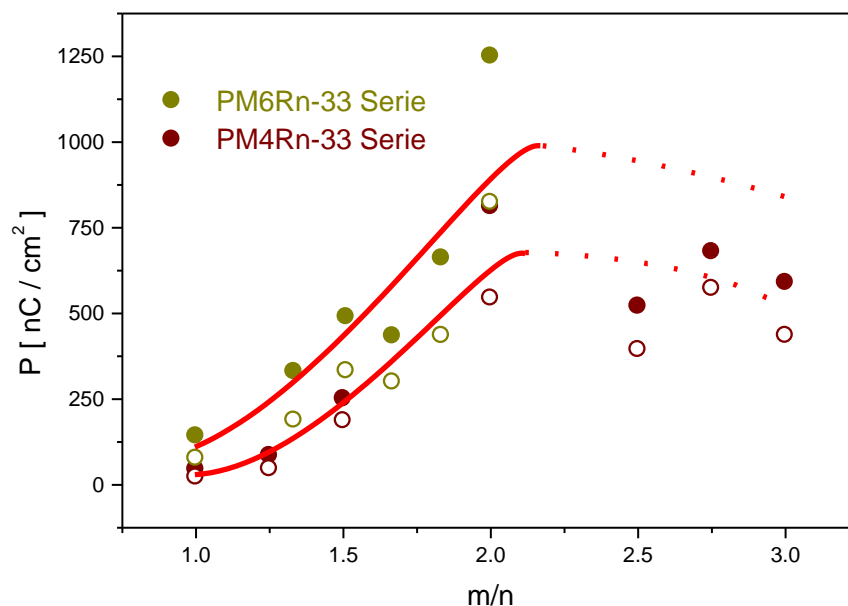
Composite Polarization

If we consider the equation $\gamma_s(T) = dP_s(T)/dT$, the polarization will arise from the integrated pyroelectric curves.





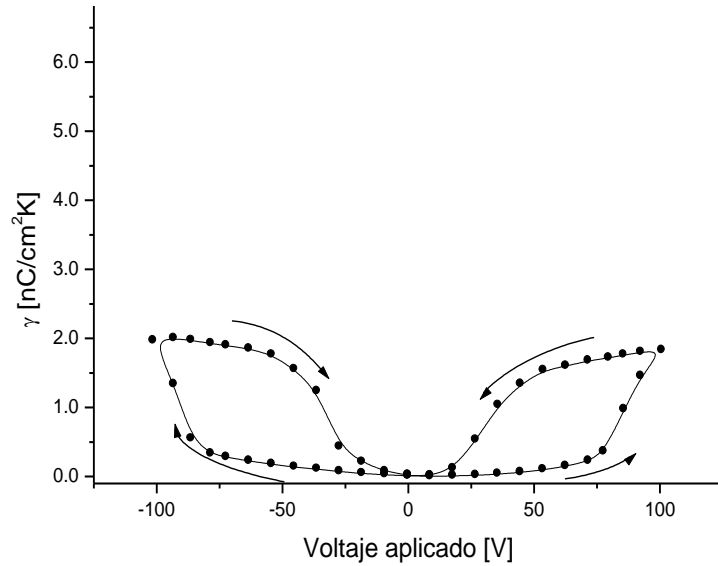
The pyroelectric response obtained focused our attention on an interesting relationship between the estimated polarization and the aliphatic chain to spacer ratio (m/n). This is reproducible for both of the homologous series, showing the largest value for PM6R12-33 in the PM6R n -33 Serie and for PM4R8-33 in the PM4R n -33 serie.



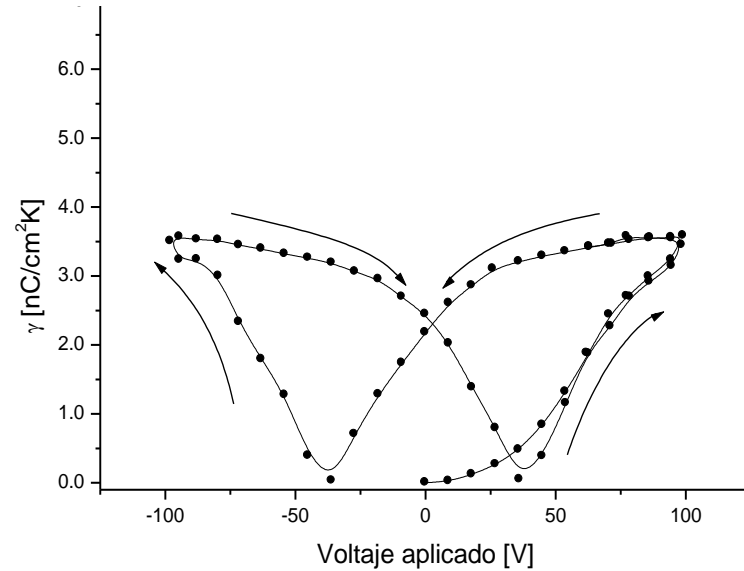
Polarisation vs alkyl chain to spacer ratio for both Series.
Open circles at 30 °C; solid circles at -170 °C.

Hysteresis loops at $T = 150^{\circ}\text{C}$

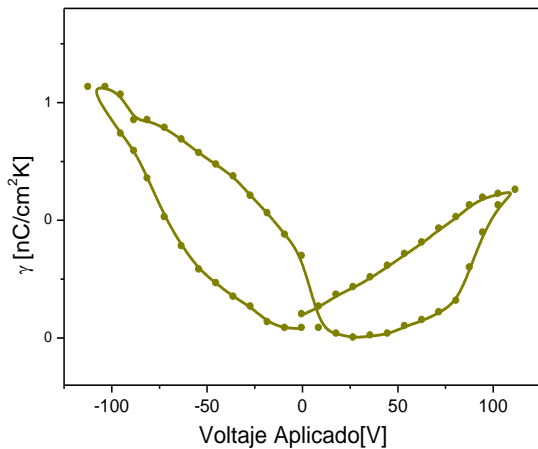
PM6R8-33



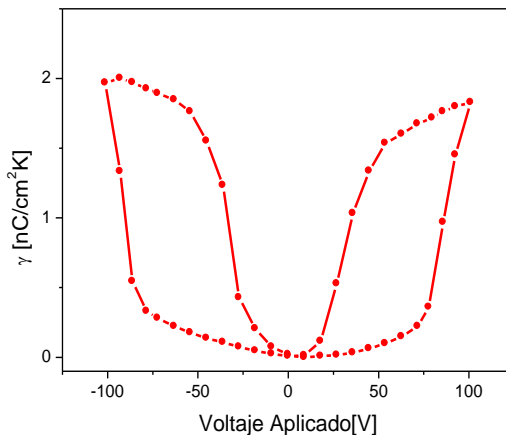
PM6R12-M4R8



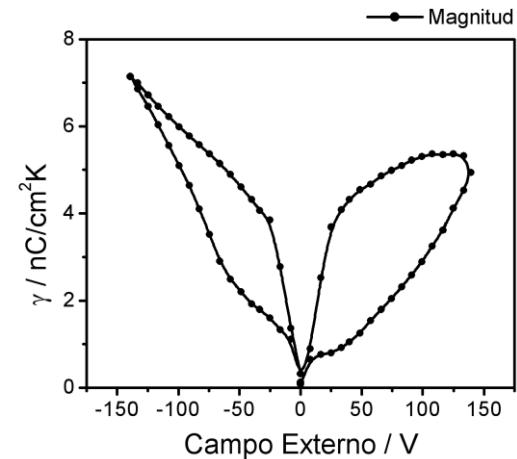
PM6R7-33



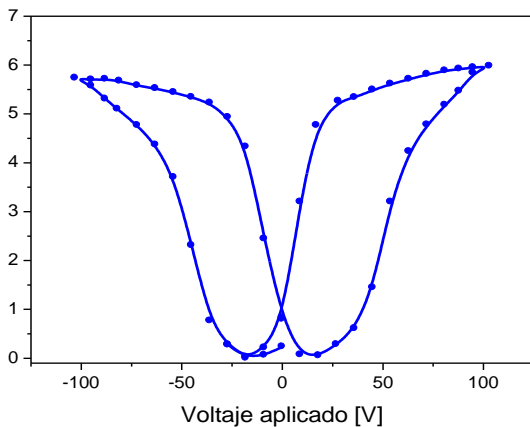
PM6R8-33



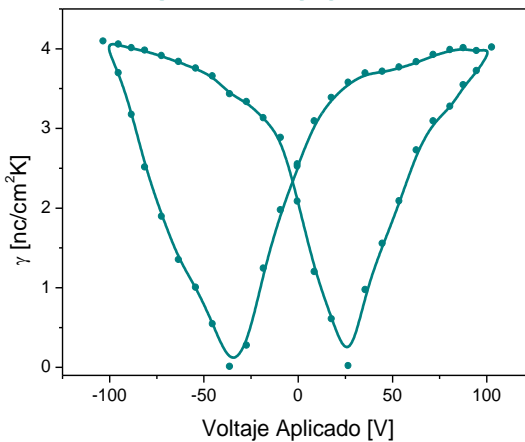
PM6R9-33



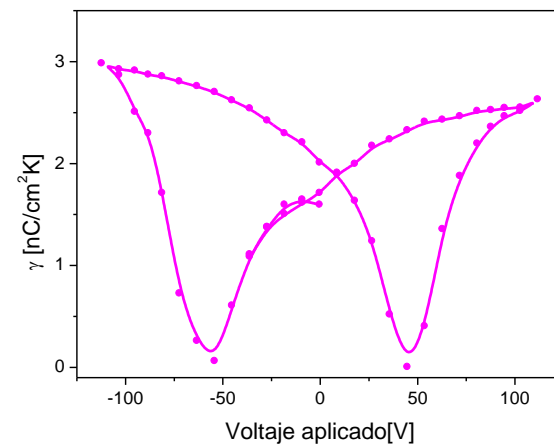
PM6R10-33



PM6R11-33



PM6R12-33



ANTIFERROELECTRIC

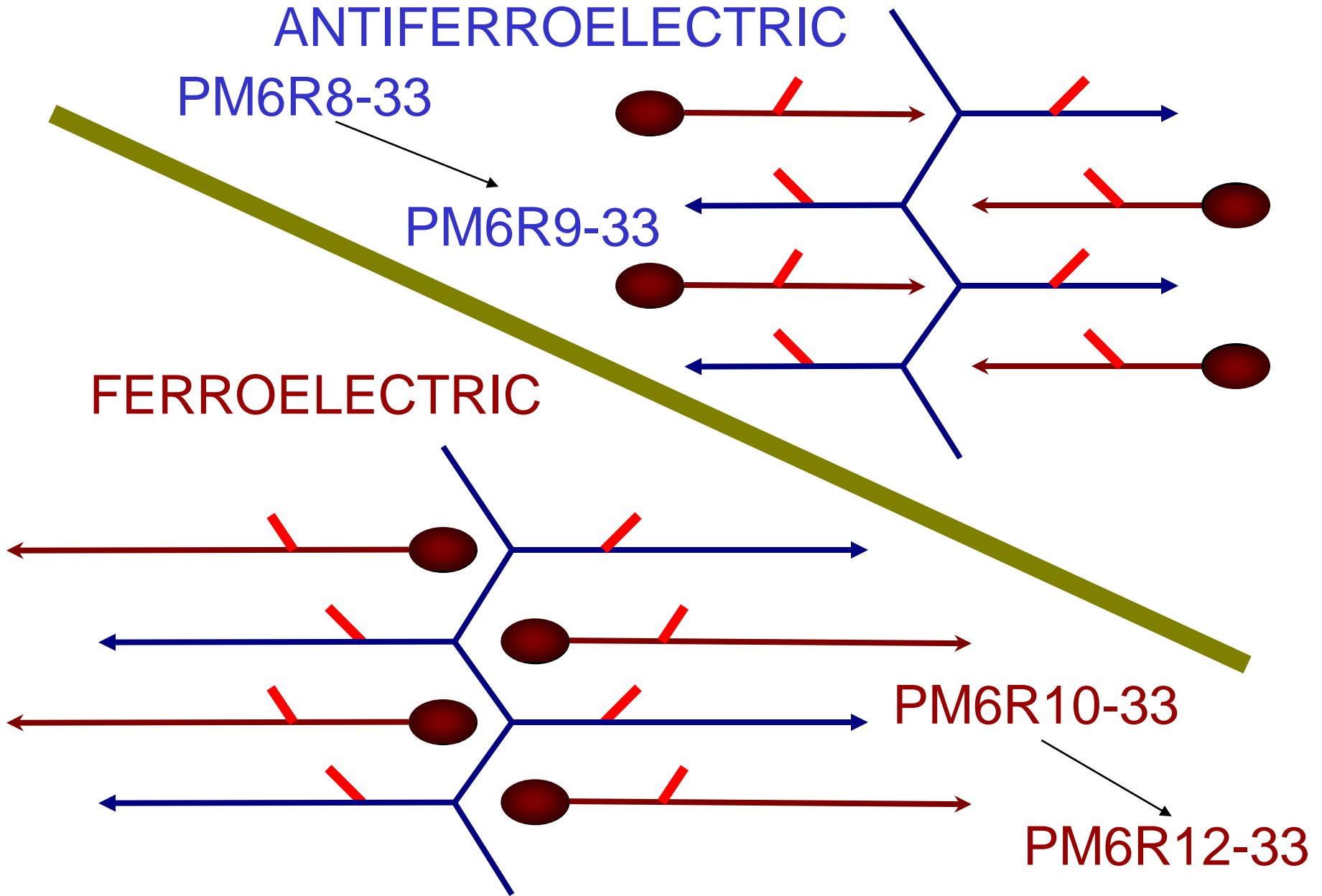
PM6R8-33

PM6R9-33

FERROELECTRIC

PM6R10-33

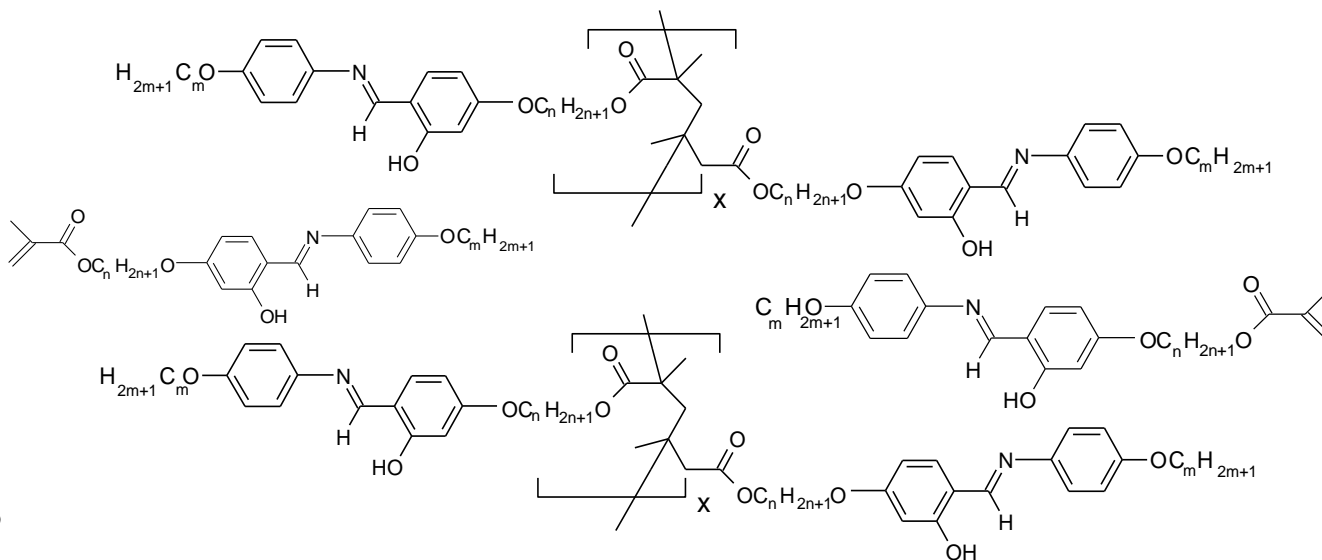
PM6R12-33



ANTIFERROELECTRIC

PM6R6-33

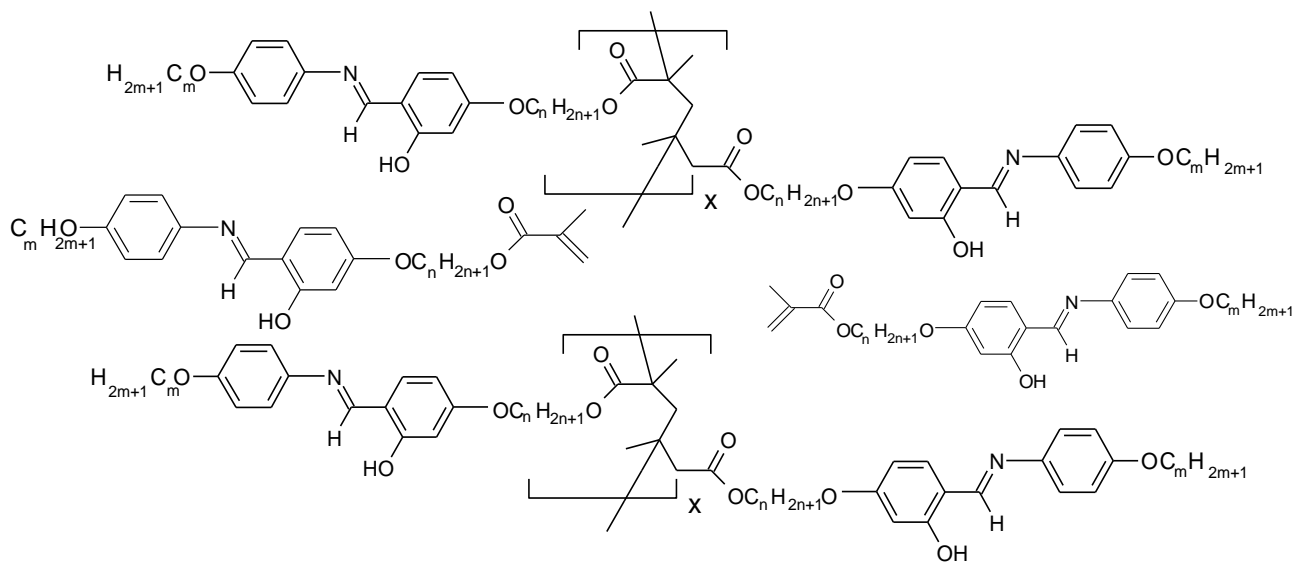
PM6R9-33



PM6R10-33

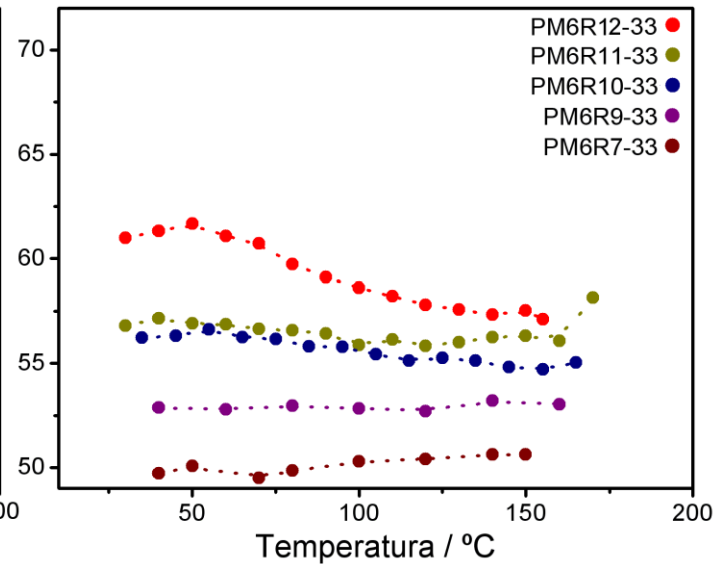
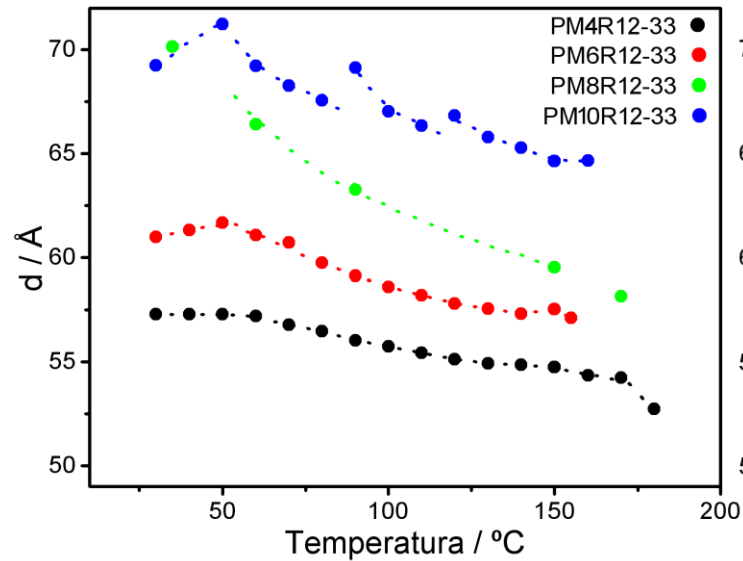
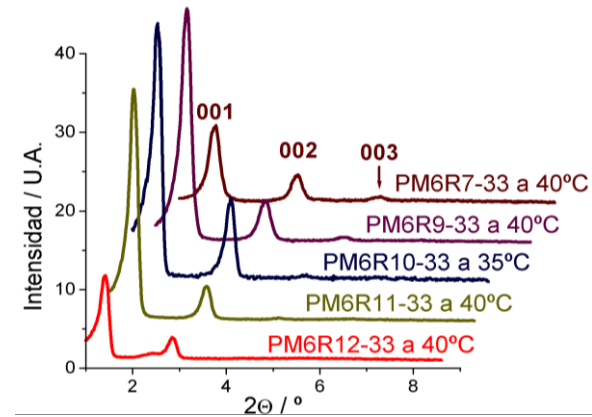
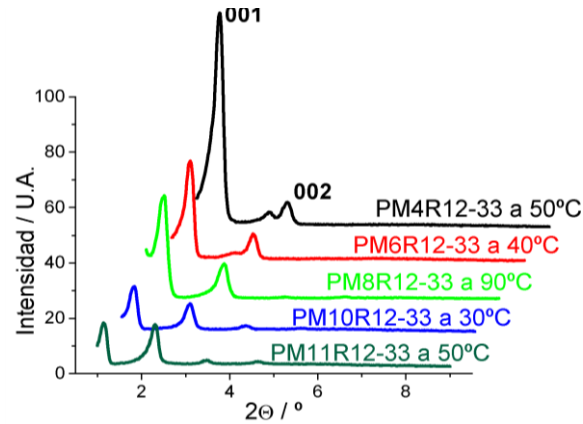
PM6R12-33

FERROELECTRIC

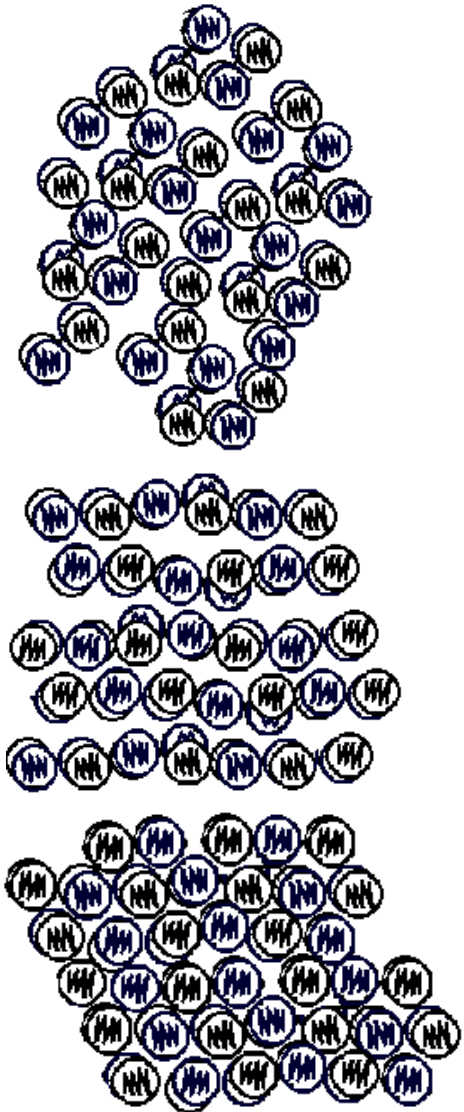
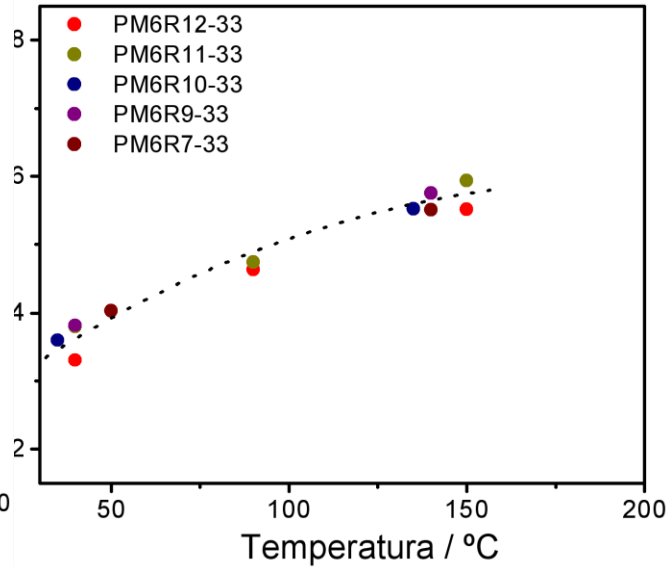
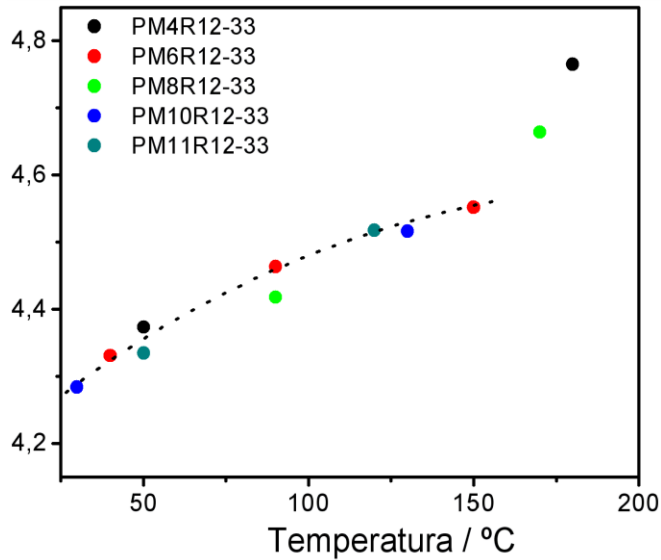
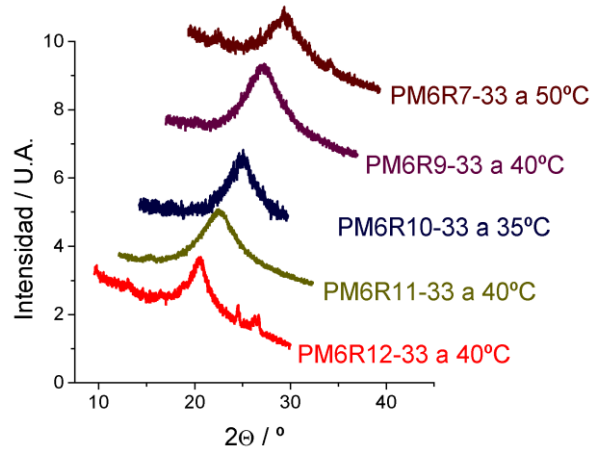
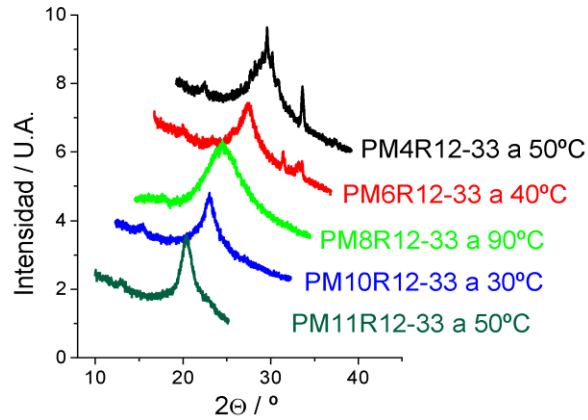


X-Ray studies in composites

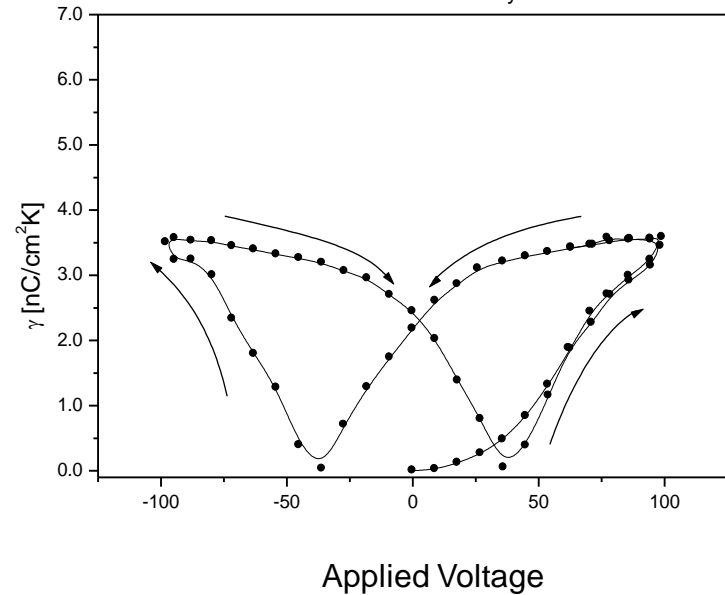
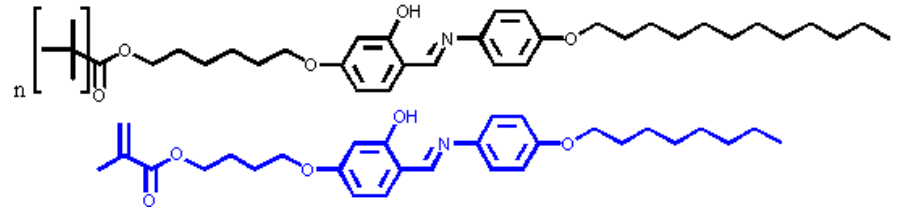
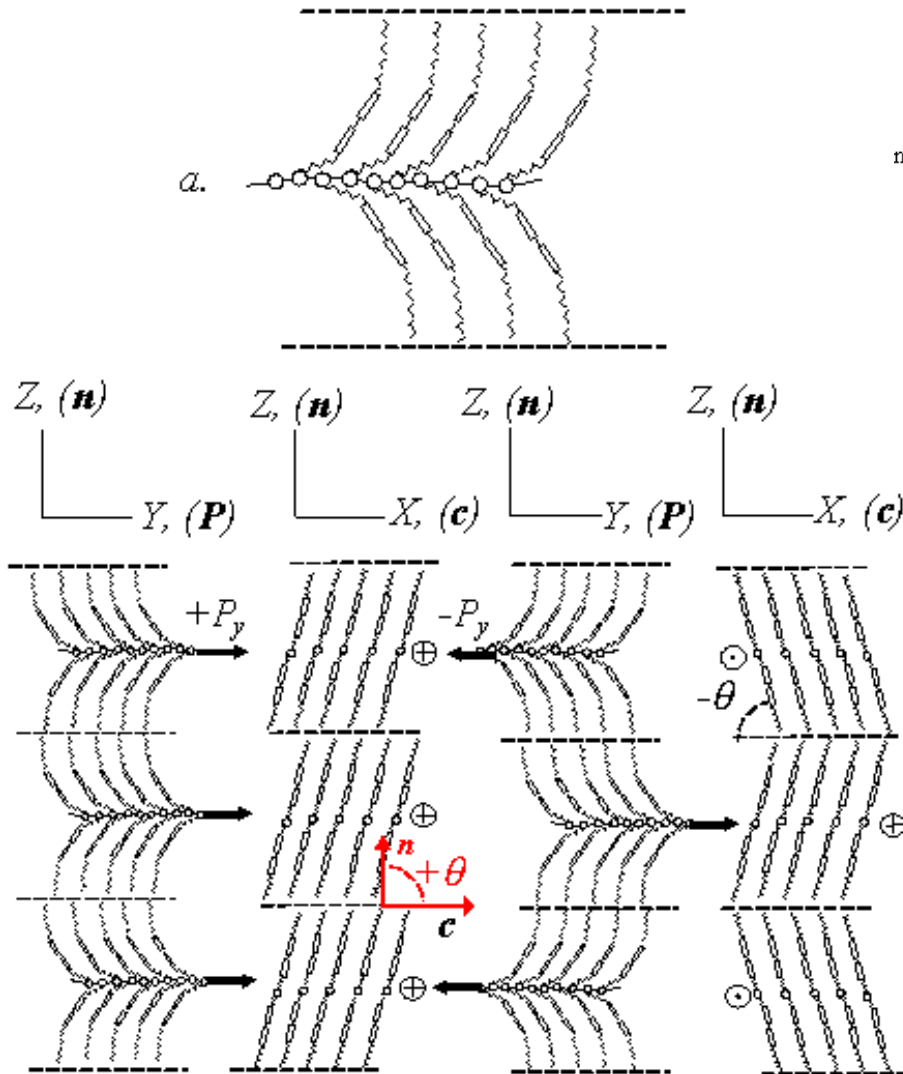
Interlayer distance: small angles reflexes



Fluidity: Wide angle reflexes

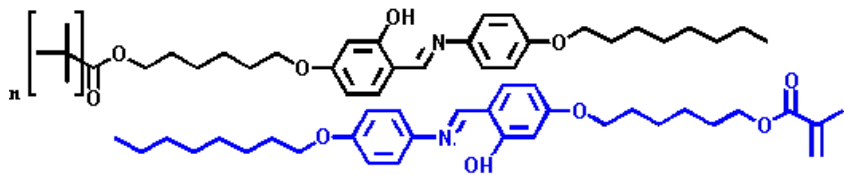


Described model for PM6R12-M4R8^[1]

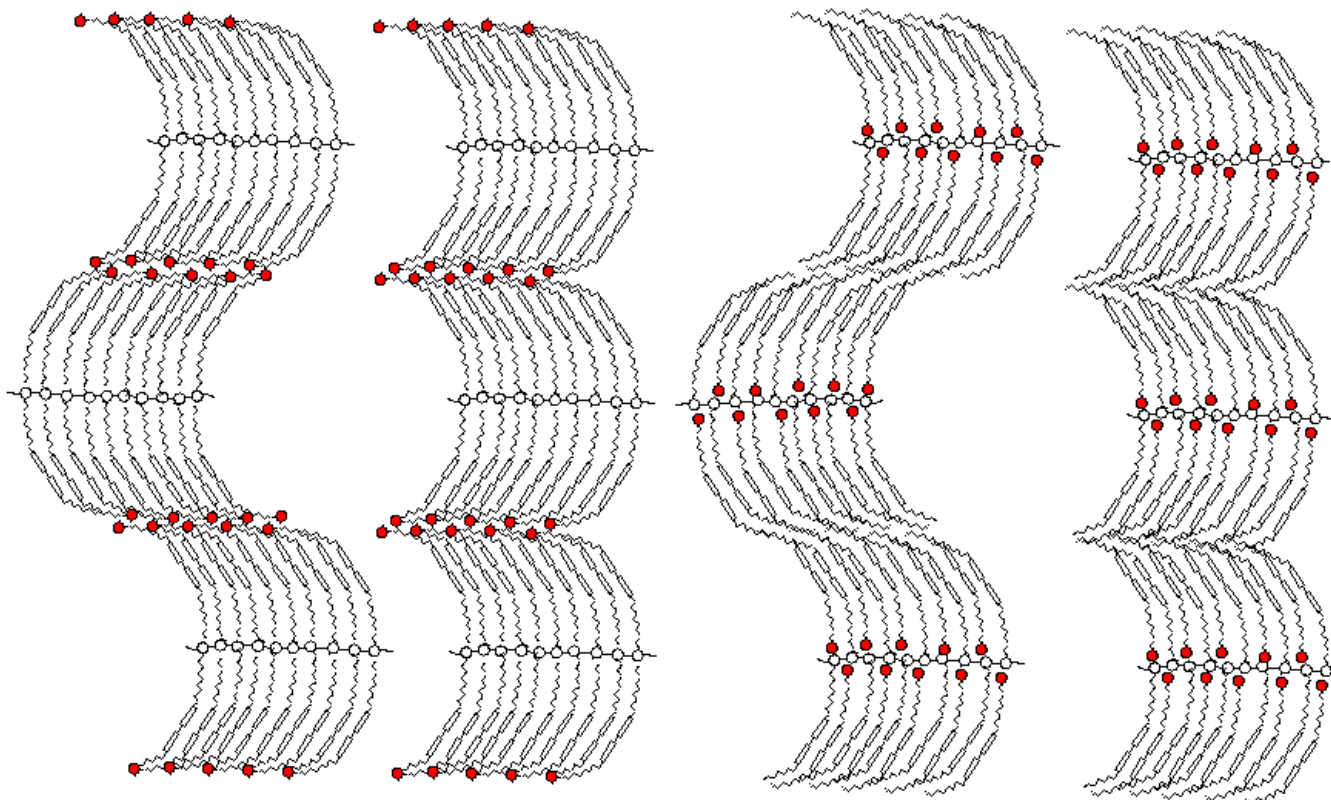
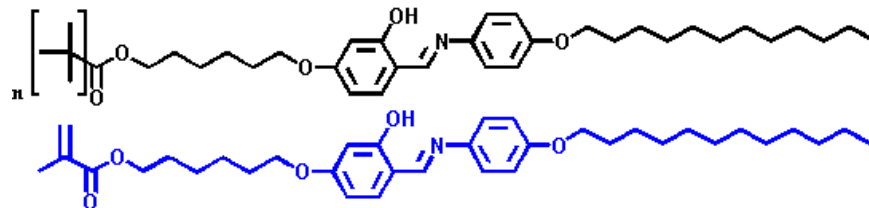


[1] S. V. Yablonskii, E. A. Soto-Bustamante*, R. O. Vergara-Toloza, W. Haase.
Ferroelectricity in Achiral Liquid Crystal Systems. Adv. Mat., 16, 1936-1940, 2004.

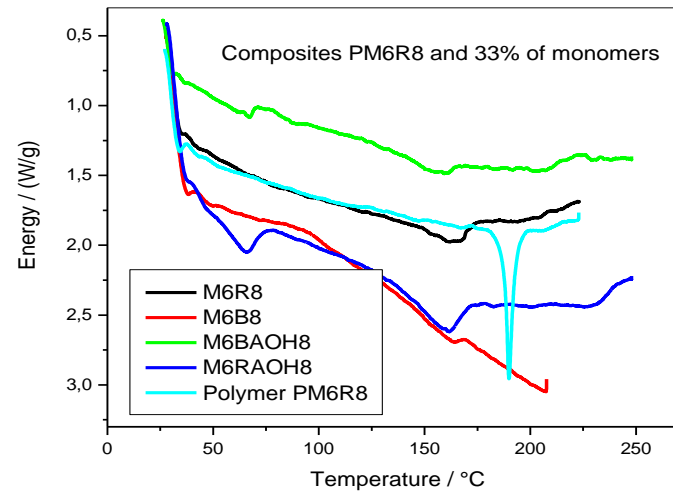
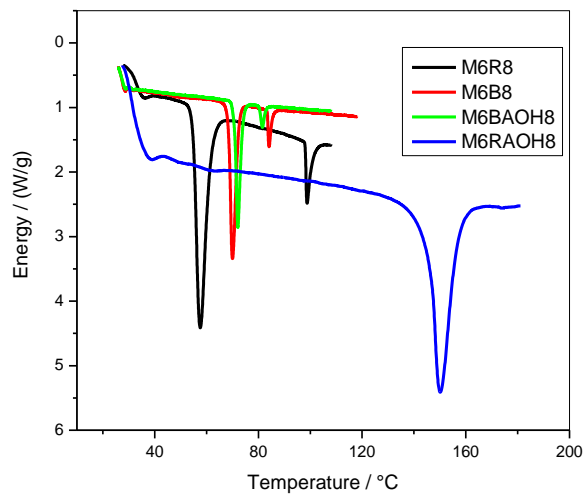
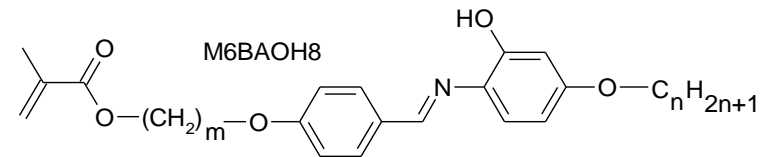
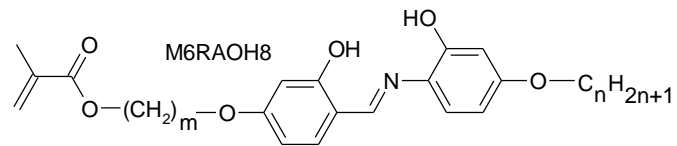
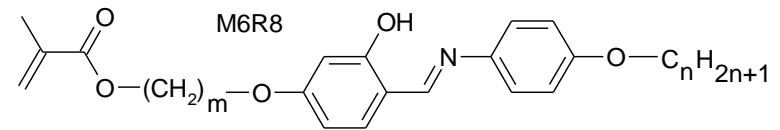
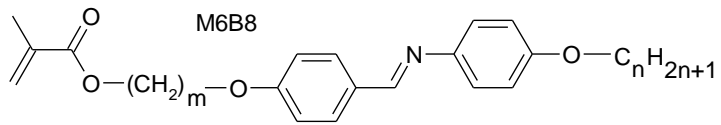
PM6R8-33%



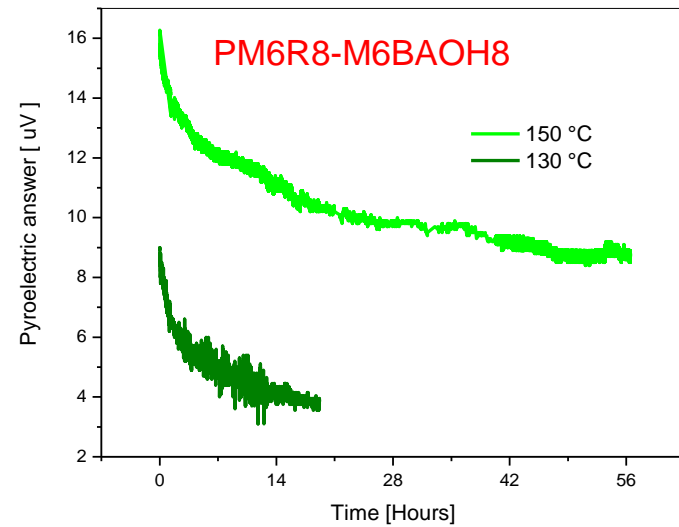
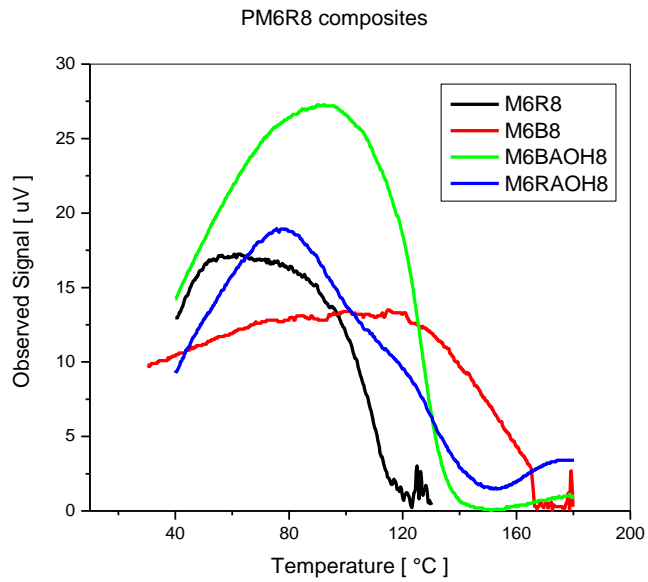
PM6R12-33%



Other systems



Pyroelectric behaviour and signal stability

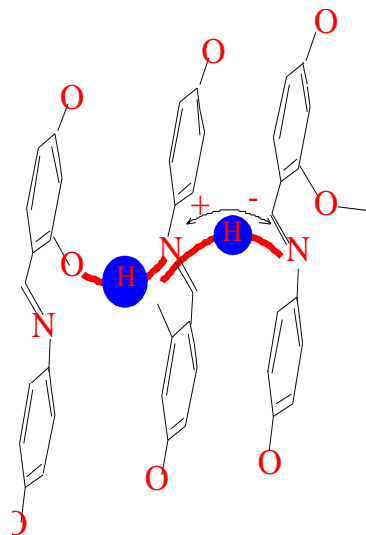
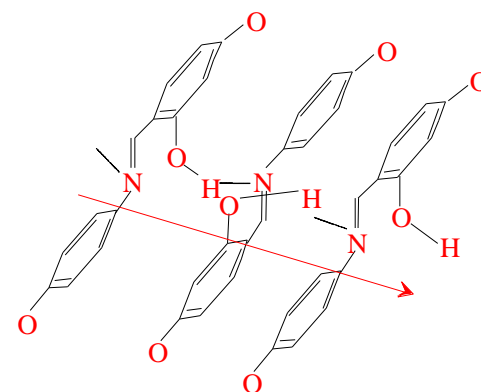
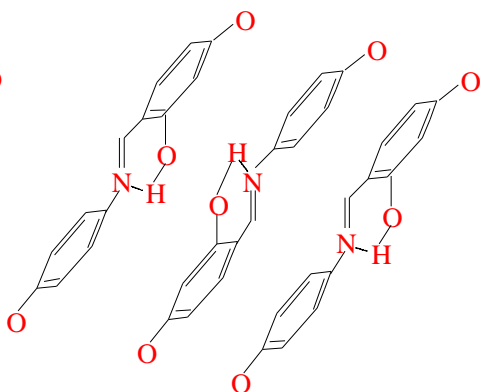
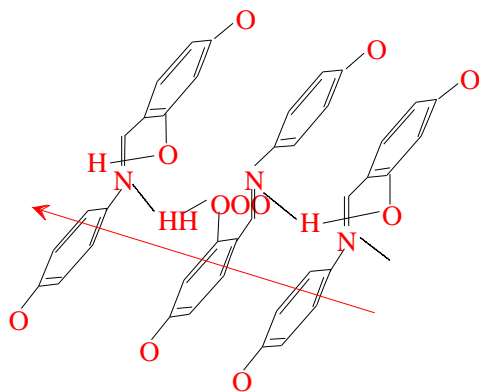


Hydrogen bonding

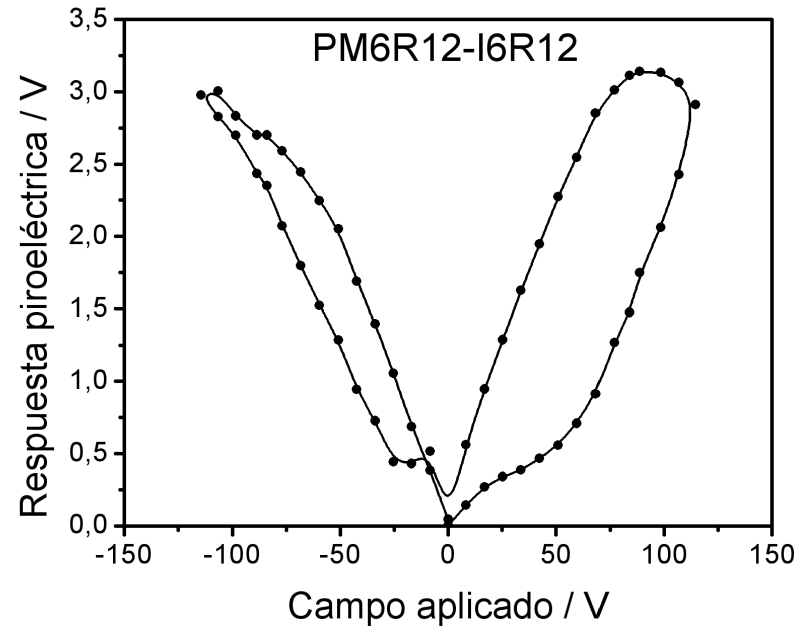
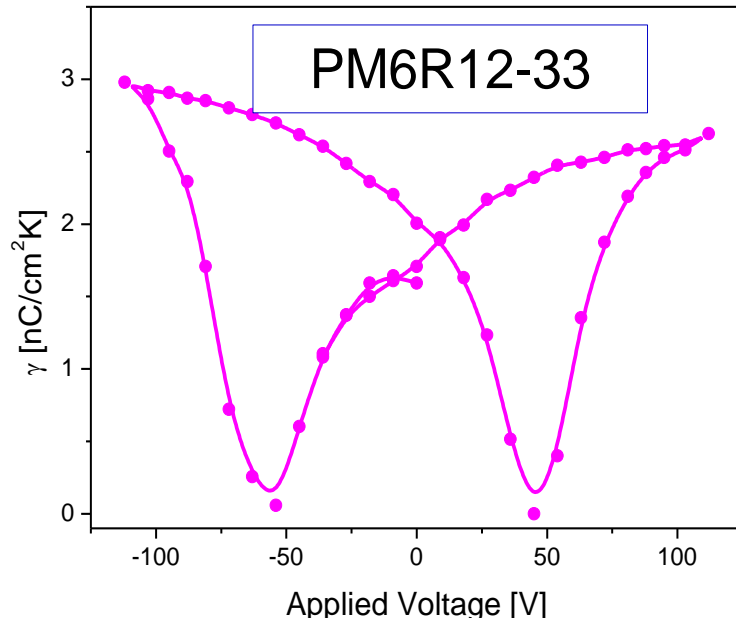
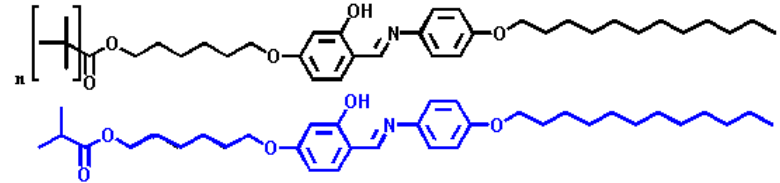
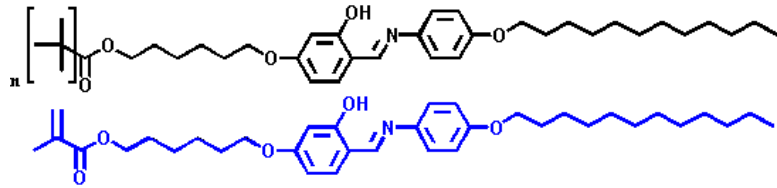
-E

E=0

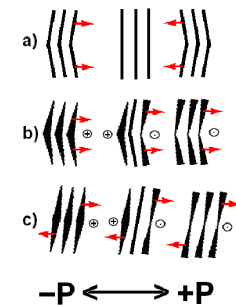
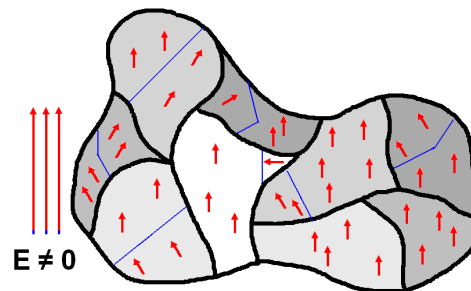
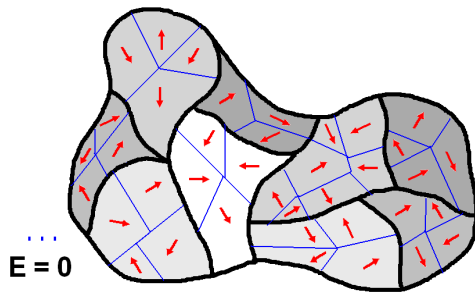
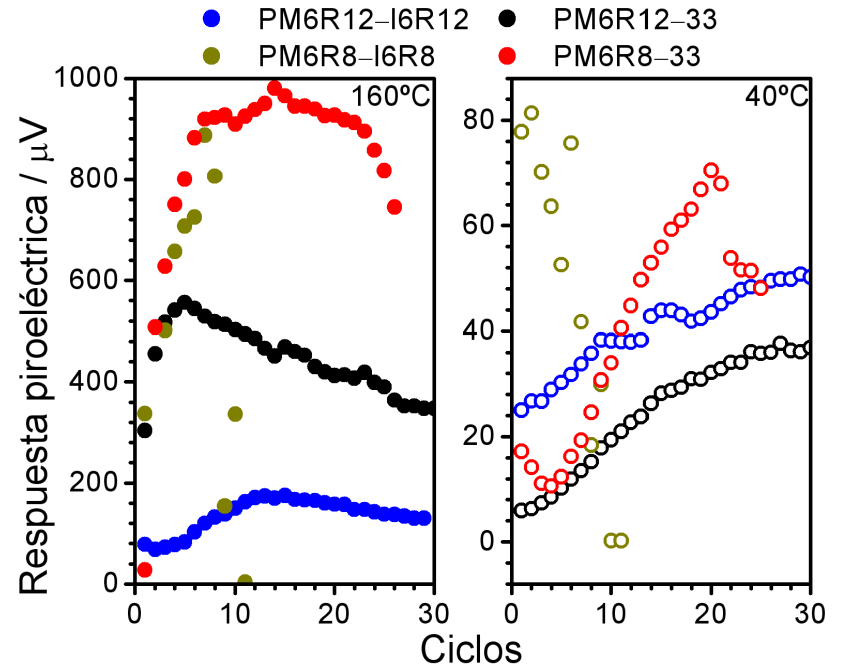
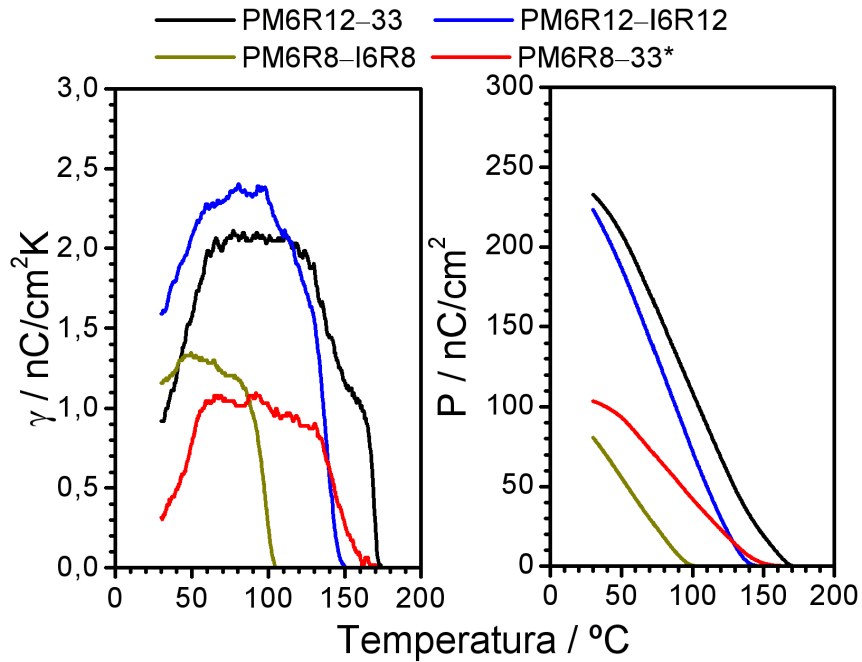
+E



PM6R12-I6R12: no methacrylic group



Signal stability



Acknowledgments

Telekom

Fundación Andes

Universidad de Chile

FONDECYT

VW-Stiftung

Pyroelectric detectors

Detector materials:

Triglycine sulfate (TGS) :

High pyroelectric coefficients

Relatively low permittivity.

Favorite for high-sensitivity applications.

Lithium tantalate:

High Stability

Insensitivity to humidity and vacuum

Used for space applications.

Polyvinylidene fluoride polymer (PVDF)

Low pyroelectric coefficients

Low thermal conductivity and dielectric constant

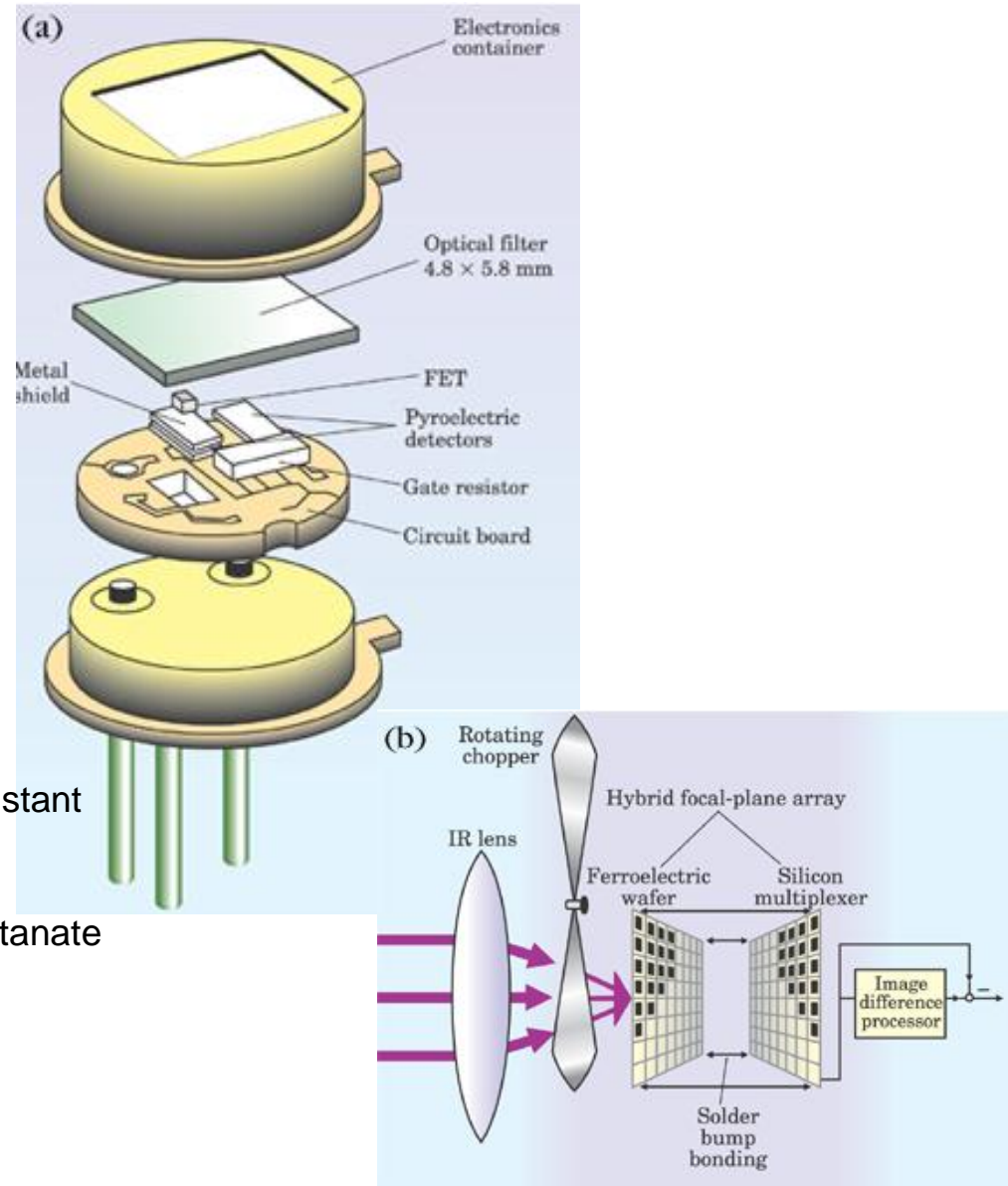
Useful for large-area detectors and arrays.

Ceramics based on the lead zirconate titanate

The most widely used materials

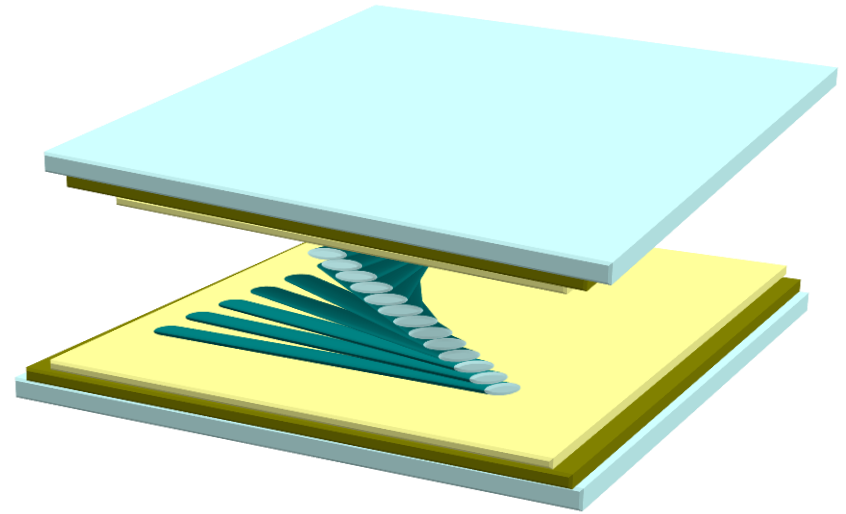
Relatively cheap to manufacture

Mechanically and chemically robust.



Development of FLC's is a well explored field in the last decade, due to their strong technological applications in liquid crystal displays.

One of the mayor task is to find a system able to align preferentially molecules with a good order degree and strong enough anchoring forces.

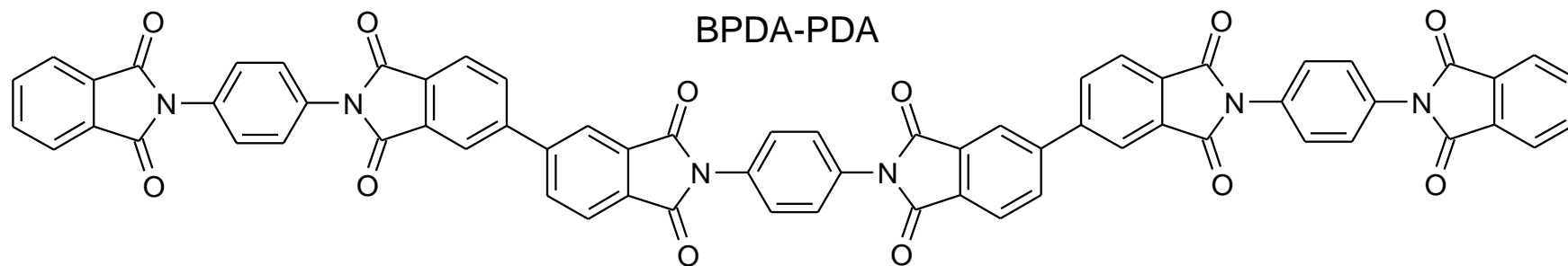


Nowadays, coated surfaces with mechanically oriented polyamide are one of the most used approach.

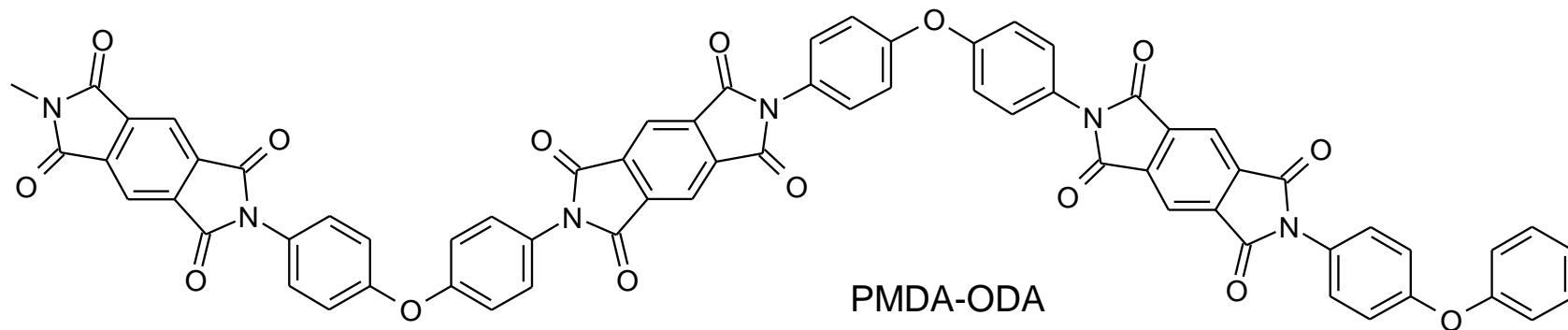
Other improvements are carried out by using fotolaignement of azodyes.

This last approach avoid generation of induced charges that later on can produce screen defects.

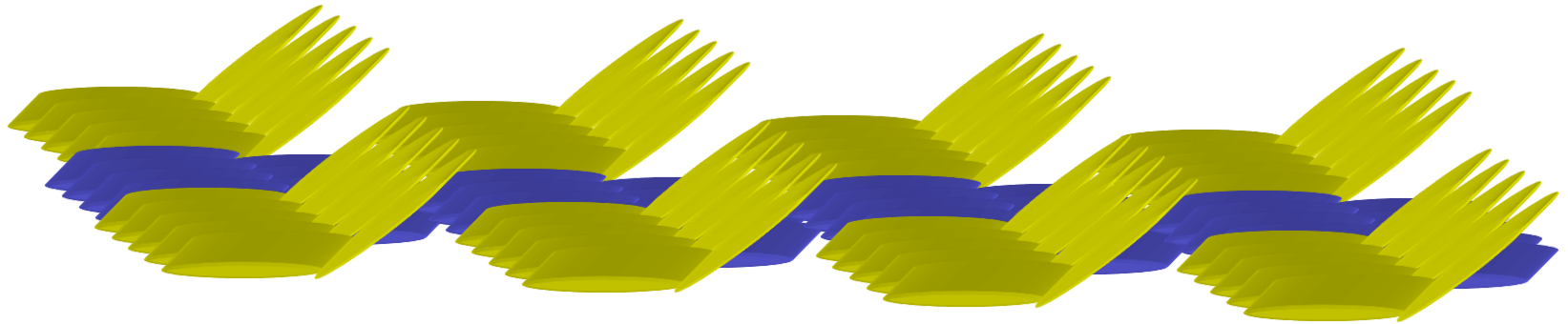
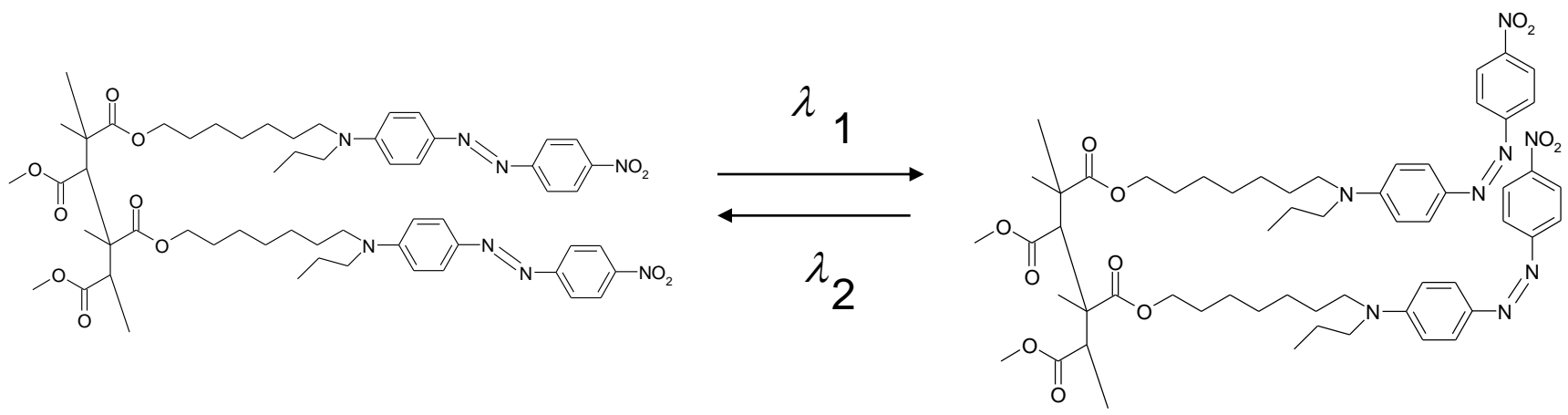
Polyamide



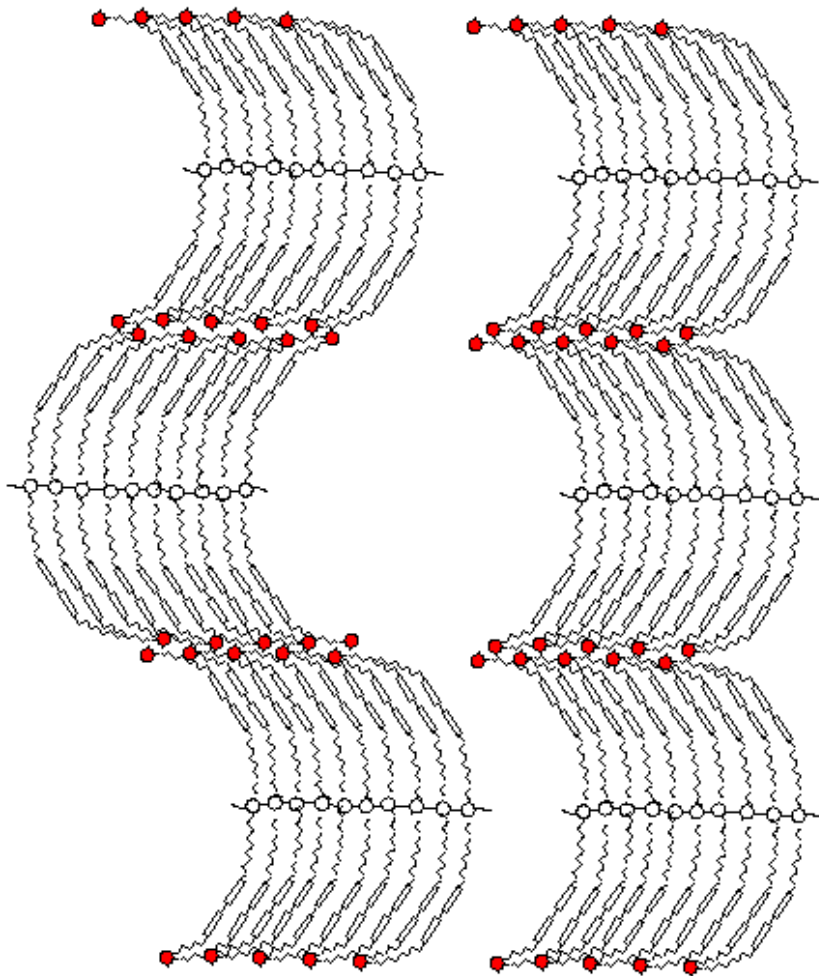
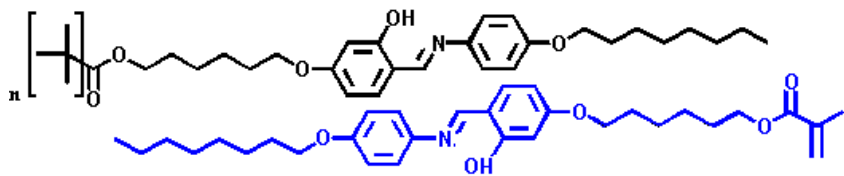
Macromolecules, **31**, 1930 (1998).



Macromolecules, **29**, (1996), 8335.



PM6R8-33%



PM6R12-33%

